



**UNIVERSIDAD AUTÓNOMA  
DE SAN LUIS POTOSÍ  
FACULTAD DE MEDICINA**



**Centro de Investigación en Ciencias de la  
Salud y Biomedicina (CICSaB)**



**EFFECTO DE LA INFECCIÓN DEL VIRUS DE ZIKA EN LA  
DIFERENCIACIÓN NEURAL DE UNA LÍNEA CELULAR  
TRONCAL HUMANA**

**TESIS QUE PRESENTA**

M. C. EDSON IVÁN RUBIO HERNÁNDEZ

PARA OBTENER EL GRADO DE  
**DOCTOR EN CIENCIAS BIOMÉDICAS BÁSICAS**

CODIRECTORES DE TESIS

**DRA. CLAUDIA CASTILLO MARTÍN DEL CAMPO  
DR. MAURICIO COMAS GARCÍA**

Marzo 2023

## **CRÉDITOS INSTITUCIONALES**

Este trabajo se llevó a cabo bajo la tutoría de la Dra. Claudia Castillo Martín del Campo y del Dr. Mauricio Comas García en el Departamento de Centro de Investigación Aplicada en Ambiente y Salud (CIAAS) de la Coordinación para la Innovación y Aplicación de la Ciencia y la Tecnología (CIACYT) y en la Sección de Microscopia de Alta Resolución del Centro de Investigación en Ciencias de la Salud y Biomedicina (CICSaB), de la Universidad Autónoma de San Luis Potosí, con la beca otorgada por el CONACYT con número (CVU) 775486.

Tesis que presenta:

**M.C. EDSON IVÁN RUBIO HERNÁNDEZ**

PARA OBTENER EL GRADO DE DOCTOR  
EN CIENCIAS BIOMÉDICAS BÁSICAS

### **CODIRECTORES DE TESIS**

DRA. CLAUDIA CASTILLO MARTÍN DEL CAMPO  
DR. MAURICIO COMAS GARCÍA

### **ASESORES INTERNOS**

DRA. ADRIANA MONSIVÁIS URENDA.  
DR. CHRISTIAN ALBERTO GARCÍA SEPÚLVEDA.

### **ASESOR EXTERNO**

DR. JOSÉ FERNANDO PEÑA ORTEGA.

### **JURADO**

#### **PRESIDENTE DE SINODALES:**

DR. DANIEL NOYOLA CHERPITEL.

#### **SECRETARIA DE SINODALES:**

DRA. ADRIANA MONSIVÁIS URENDA.

#### **SINODALES:**

DRA. DIANA PATRICIA PORTALES PÉREZ.

DR. JOSÉ FERNANDO PEÑA ORTEGA.

#### **SINODAL SUPLENTE:**

DRA. SARAY ARANDA ROMO

Marzo 2023





**Efecto de la infección del virus de Zika en la diferenciación neural de una línea celular troncal humana.** Por Edson Iván Rubio Hernández. Está licenciado bajo una [Licencia Creative Commons Reconocimiento-NoComercial-CompartirIgual 4.0 Internacional](https://creativecommons.org/licenses/by-nc-sa/4.0/) .

## AGRADECIMIENTOS

Quiero agradecer a mi comité de tesis, tanto a mis directores de tesis: Dra. Claudia y Dr. Mauricio, y a mis asesores: Dr. Christian, Dra. Adriana y Dr. Fernando, por compartir su conocimiento conmigo durante cada seminario. Su disposición y buena actitud en los seminarios serán uno de los mejores recuerdos de mi doctorado.

Agradezco de manera especial y sincera a mi codirectora de tesis, Dra. Claudia, por aceptarme en su laboratorio desde el año 2015. La confianza depositada en mí ha hecho que crezca de forma profesional y académica.

Reconozco a mis codirectores de tesis, Dra. Claudia y Dr. Mauricio, por proporcionarme los medios para llevar a cabo todos los experimentos que respaldan esta tesis doctoral.

Quiero expresar también mi mayor agradecimiento a los señores Nazario Rubio Perales y Juana Hernández Martínez, mis padres, a quienes les debo todo. Gracias a la confianza que siempre han puesto en mí y la ayuda que me han proporcionado. Siempre estaré orgulloso de ustedes.

A Moisés Gámez por el acompañamiento y apoyo en todo momento.

Y a mis nuevos y viejos amigos (Gabriela, Arleth, Rebeca, Ariana, por nombrar algunos), que me acompañaron en todo momento. La experiencia académica, de compañerismo y amistad que tuve durante estos cuatro años tanto en la UASLP como en mi estancia de investigación en el Hospital Infantil de México Federico Gómez, me hace sentir afortunado.



# **Astrocytes derived from Neural Progenitor Cells are susceptible to Zika Virus Infection.**

**Edson I. Rubio-Hernández<sup>1</sup>; Miguel A. Coronado-Ipiña<sup>2</sup>; Mayra Colunga-Saucedo<sup>3</sup>; Hilda M. González Sánchez<sup>4</sup>; Mauricio Comas-García<sup>2,5\*</sup>; Claudia G. Castillo-Martín del Campo<sup>1\*</sup>**

<sup>1</sup> *Laboratorio de Células Troncales Humanas, Coordinación para la Innovación y Aplicación de la Ciencia y la Tecnología-Facultad de Medicina, Universidad Autónoma de San Luis Potosí, San Luis Potosí, México*

<sup>2</sup> *Sección de Microscopia de Alta Resolución, Centro de Investigación en Ciencias de la Salud y Biomedicina, Universidad Autónoma de San Luis Potosí, San Luis Potosí, México*

<sup>3</sup> *Sección de Genómica Médica, Centro de Investigación en Ciencias de la Salud y Biomedicina, Universidad Autónoma de San Luis Potosí, San Luis Potosí, México*

<sup>4</sup> *Cátedra CONACYT- Centro de Investigación sobre Enfermedades Infecciosas, Instituto Nacional de Salud Pública, Cuernavaca, México*

<sup>5</sup> *Facultad de Ciencias, Universidad Autónoma de San Luis Potosí, San Luis Potosí, México.*

*\* Corresponding author*

*E-mail: mauricio.comas@uaslp.mx. (MCG)*

*\* Corresponding author*

*E-mail: claudia.castillo@uaslp.mx. (CGCMC)*

# ABSTRACT

Zika virus (ZIKV) was first isolated in 1947. From its isolation until 2007, symptoms of ZIKV-caused disease were limited (e.g., fever, hives, and headache); however, during the epidemic in Brazil in 2014, ZIKV infection caused Guillain-Barré syndrome in adults and microcephaly in fetuses and infants of women infected during pregnancy. The neurovirulence of ZIKV has been studied using neural progenitor cells (NPCs), brain organoids, neurons, and astrocytes. NPCs and astrocytes appear to be the most susceptible cells of the Central Nervous System to ZIKV infection. In this work, we aimed to develop a culture of astrocytes derived from a human NPC cell line. We analyze how ZIKV affects human astrocytes and demonstrate that 1) ZIKV infection reduces cell viability, increases the production of Reactive Oxygen Species (ROS), and results in high viral titers; 2) there are changes in the expression of genes that facilitate the entry of the virus into the cells; 3) there are changes in the expression of genes involved in the homeostasis of the glutamatergic system; and 4) there are ultrastructural changes in mitochondria and lipid droplets associated with production of virions. Our findings reveal new evidence of how ZIKV compromises astrocytic functionality, which may help understand the pathophysiology of ZIKV-associated congenital disease.

**KEYWORDS:** Zika virus, congenital infection, astrocytes, TAM receptors, lipid droplets, mitochondria, GFAP, glutamate.

# INTRODUCTION

Zika virus (ZIKV) is a positive-sense single-stranded RNA [(+)ssRNA] virus that belongs to the *Flaviviridae* family and *Flavivirus* genus [1, 2]. ZIKV was first isolated, in the Zika forest in Uganda in 1947 from a *Rhesus* macaque that developed a febrile illness [3]. Since its isolation and until 2007, only a dozen cases were reported world-wide. However, in 2007, 2013, and 2014 large outbreaks occurred on Yap Island (Micronesia), French Polynesia, and Brazil, respectively. Disease symptoms were similar to those caused by other arboviruses such as dengue virus (DENV), including fever, rash, and headache [4-6]. However, during the epidemic in Brazil in 2014 ZIKV infection was associated to more severe symptoms, such as Guillain-Barre Syndrome in adults and congenital malformations, fetal death and microcephaly in fetuses and infants of women infected by ZIKV during pregnancy [1].

Currently, two different genotypes of ZIKV have been identified, the African and Asian lineages [5]. The Asian lineage is the one that spread in America from Brazil and is responsible for the congenital disabilities and Guillain-Barré syndrome [5, 6]. There are many other neurodevelopmental disorders associated with ZIKV infection, e.g., ventriculomegaly, intracranial calcifications and ventricular atrophy, but microcephaly is the most common [7, 8].

It is now well recognized that ZIKV infection impairs the development of the Central Nervous System (CNS) [1, 9, 10]. In pregnant women, these neurodevelopmental disorders are more prevalent when infection happens during the first trimester of pregnancy [11, 12]. The effects of ZIKV infection on the CNS have been studied *in vitro* using neural progenitor cells (NPCs) [13-19], brain organoids [14, 19-21], neurons [22-25], and astrocytes [26-30]. In most cases,

NPCs and astrocytes are the cells more susceptible to infection by ZIKV [31]. In these cellular models, ZIKV infection compromises cell proliferation [32], induces cell death [15-17], and alters differentiation [13, 14, 33, 34].

Astrocytes are the most abundant cells in the brain, they support and maintain neuron function, contribute to homeostasis, and are a crucial defense mechanism against pathogens [35, 36]. ZIKV infection compromises their viability [28, 30], induces mitochondrial dysfunction [27], and favors an inflammatory state [29, 37]. However, we know significantly less about ZIKV infection of astrocytes than of NPCs and neurons. A significant limitation in the analysis of ZIKV infection in human astrocytes is the lack of non-cancerous cultures. Furthermore, those astrocytes available have not been properly characterized (e.g., their karyotypes, mutational burden, signaling pathways affected, clonal heterogeneity, etc.).

The human neural progenitor cell line (hNS-1) is an attractive alternative to generate astrocyte cultures. It was isolated from a 10.5-week-old human neural fetal tissue that was immortalized with a retroviral vector encoding a v-myc fusion protein [38]. hNS-1 cells proliferate in the presence of basic Fibroblast Growth Factor (bFGF) and Epidermal Growth Factor (EGF) [38-40]. Under these conditions, hNS-1 cells are multipotent and proliferate in a no-differentiated state. After the removal of these growth factors they readily differentiate into neurons, astrocytes, and oligodendrocytes, leaving a remnant of no-differentiated neural progenitors. Moreover, hNS-1 cells have a stable karyotype and do not have major structural modifications.

In this study, we generated human astrocyte cultures from hNS-1 cells (astrocytes-hNS1), characterized by the expression of *bona fide* astrocyte markers: glial fibrillary acidic protein (GFAP), the excitatory amino acid transporters type 1 and type 2 (EAAT1 and EAAT2), and glutamine synthetase (GS). We infected astrocytes-hNS1 cultures finding that ZIKV lowers

cell viability, increases the production of Reactive Oxygen Species (ROS), and yields high viral titers. We show that ZIKV modifies the expression of genes essential for CNS homeostasis, such as GFAP, EAAT1, GS, and the N-Methyl-D-Aspartate Receptor (NMDA<sub>R</sub>), and also of genes that facilitate viral entry. Thin-section Transmission Electron Microscopy (TEM) analysis of infected cells shows viral factories and the ultra-structural modifications that result in the cytopathic effect of the infected cells. These findings significantly increase our understanding of the pathogenic mechanisms of ZIKV infection in the CNS and also provide the foundation of a model for further characterization.

## **METHODS**

### **Propagation of the neural progenitor hNS-1 cells**

The human neural progenitor cell line (hNS-1) can be differentiated into neurons, astrocytes, and oligodendrocytes by modifying the proliferation media according to previously published protocol [38]. Briefly, the hNS-1 cells were cultured in poly-L-lysine-treated culture dishes (Sigma-Aldrich, St. Louis, MO) with DMEM-F12 culture medium (Gibco, Invitrogen Life Technologies, Carlsbad, CA) supplemented with 6% glucose, NDiff Neuro-2 Medium Supplement 1X (Merck-Millipore, Darmstadt, Germany), AlbuMAX I 0.5% (Gibco), basic Fibroblast Growth Factor (bFGF, R&D Systems) and Epidermal Growth Factor (EGF, R&D Systems). This cell line was donated by Dr. Alberto Martinez-Serrano at the "Severo Ochoa" Molecular Biology Center, Madrid, Spain.

### **Isolation of human astrocytes**

The hNS-1 cells were differentiated for 21 days, by removing the growth factors and by adding 0.5% Fetal Bovine Serum (FBS, Sigma-Aldrich), then they were harvested using

trypsin with 0.5% EDTA (Sigma) and seeded in culture dishes not treated with poly-L-lysine [41, 42]. The culture was maintained with DMEM Medium (Gibco) supplemented with 10% FBS, 100 U/ml Penicillin, 100 µg/mL Streptomycin, and non-essential amino acids (110 µM L-Alanine, 100 µM L-asparagine, 100 µM L-aspartic acid, 100 µM L-glutamic acid and 100 µM proline). The medium was replaced daily to remove non-adherent cells (e.g., neural progenitors and neurons), and the cells were harvested when they reached a 95% confluency. The generated cultures were designated astrocytes-hNS1; these had at least five passages in which non-adherent cells were no longer observed using bright field microscope with a 10x objective. The cultures were maintained at 37°C, 95% humidity, and 5% CO<sub>2</sub>.

## **Characterization of astrocytes-hNS1**

### *GFAP immunofluorescence*

The identity of the astrocytes-hNS1 was confirmed by immunofluorescence against GFAP, a marker routinely used to identify glial cells [42]. Astrocytes-hNS1 were seeded in 24-well plates with coverslips at  $6 \times 10^4$  cells per well. After three days, the culture medium was removed, and the samples were recovered for immunofluorescence as previously described [40, 43]. Briefly, cells were washed with phosphate buffer (PBS, 138 mM NaCl, 3 mM KCl, 8.1 mM Na<sub>2</sub>HPO<sub>4</sub>, and 1.5 mM KH<sub>2</sub>PO<sub>4</sub>) and fixed with 4% paraformaldehyde (PFA) for 10 minutes at room temperature. Then the cells were washed three times with PBS, treated with 0.05% sodium borohydride (Sigma-Aldrich) for 10 minutes, washed three times with 0.25% Triton X-100 (Sigma-Aldrich) in PBS, and blocked with 20% Horse Serum (Gibco) in PBS for 2 hours. Subsequently, the cells were incubated with the primary rabbit anti-GFAP antibody (1:1000, Cat. No. Z033401, Dako) overnight at 4°C, cells were then washed twice with 0.25% Triton X-100 1% and horse serum in PBS, and incubated with the secondary

antibody (Alexa-546 goat anti-rabbit a 1:300 dilution, Cat. No. A-11010, Invitrogen) for 2 hours at room temperature. The nuclei were stained with Hoechst 33258 (0.2 µg/ mL, Invitrogen) for 10 minutes, washed four times with PBS, and the coverslips were mounted with Vectashield mounting medium (Vector labs). The cells were analyzed in the LEICA DM2500 epifluorescence microscope with the filter cube A (BP:340-380), cube I3 (BP:450-490, 510), and cube N2.1 (BP:515-560, 580). A total of 7-8 fields per coverslip were captured, 3-4 coverslips were analyzed per independent experiment, and four independent experiments were performed.

#### *RT-PCR of GFAP*

Onto 6-well plates,  $5 \times 10^5$  cells per well were seeded and allowed to proliferate for three days. The total cellular RNA was obtained on the third day using Trizol™ (Life Technologies, Rockville, MD), following the supplier's instructions. The expression of the glial marker *GFAP*, was determined by one-step endpoint RT-PCR using the OneStep RT-PCR kit (Qiagen, Cat. No. 210212) according to the supplier's instructions. Using 50 ng of RNA in a reaction volume of 25 µL, PCR was performed under the following conditions: Reverse transcription at 50°C for 30 minutes; activation of DNA polymerase at 95°C for 15 minutes; 30 cycles of denaturation at 94°C for 30 seconds, alignment at 60°C for 30 seconds, and extension at 72°C for 1 minute; and a final extension at 72°C for 10 minutes. The amplification products were visualized on a 1% agarose gel. The sequences of the primers used, and the size of the amplicon are depicted in Table S1.

## **Analysis of the karyotype**

The karyotype of the astrocytes-hNS1 was analyzed to determine their genomic integrity in culture. Briefly,  $2.5 \times 10^5$  cells per well were seeded in 6-well plates and allowed to proliferate for two days. The cells were washed with PBS and incubated with colchicine (1 µg/mL) for

2 hours at 37°C, then the colchicine was removed, and the cells were washed once with PBS and harvested with trypsin. The cells were centrifuged at 1500 rpm for 5 minutes, and the pellet was resuspended in 1.5 mL of fresh medium, 10 mL of warmed hypotonic solution (75 mM KCl) were added dropwise and the cells were incubated for 20 minutes at 37°C. The cells were centrifuged at 2000 rpm for 10 minutes, the supernatant was eliminated, leaving 1 ml behind and flicking the pellet. Next, 10 ml of ice-cold fresh fixative solution (75% methanol and 25% acetic acid) was added, the cells were centrifuged for 5 minutes at 2000 rpm. This step was repeated twice. The cellular pellet was resuspended in 1 ml of fixative solution and poured onto cold slides. The sample was allowed to dry at room temperature, and fixation was performed using heat. The next day the samples were stained for 10 minutes with 0.4% Giemsa (Sigma-Aldrich), followed by washes with 4% ethanol in water and pure water. The metaphases were observed under a Motic microscope with the 100X objective.

## **Viral propagation, production of stocks and infections**

ZIKV infectious viral particles were obtained by transfecting HEK-293T cells with an infectious cDNA that contained a full-length clone of ZIKV isolated from the 2015 epidemic in Brazil [44]. The ZIKV-ICD plasmid (GenBank: KX576684.1) was donated by Dr. Alexander Pletnev from NIAI/NIH. This plasmid was transfected into HEK-293T cells using the calcium phosphate method [45]. Viral stocks were obtained by infecting Vero E6 cells with the supernatant of the transfected cells. The viral titers were determined by plaque assay using Vero E6 cells as described previously [29]. For infections of the astrocytes-hNS1, cells were seeded, washed twice with serum-free medium, and the viral inoculum was set at the desired multiplicity of infection (0.1 and 1 MOI). The inoculum was incubated for 2 hours, shaking every 10 minutes prior to being removed. The cells were washed once with serum-free



medium, and a fresh medium was added to maintain the culture until the required post-infection times.

## **Viral production kinetics and percentage of infected cells**

Viral production was analyzed by seeding  $5 \times 10^5$  astrocytes-hNS1 per well in 6-well plates, and 24 hours later were infected at a MOI of 1. The culture was maintained for five days post-infection (dpi), one-third of the medium was replaced by a fresh medium every 24 hours, and the removed media was stored at  $-80^\circ\text{C}$  until quantification of viral load.

To determine the percentage of infected cells,  $6 \times 10^4$  cells per well were seeded in 24-well plates and infected at a MOI of 1 at 24 hours post-seeding. At three dpi, the cells were analyzed by immunofluorescence using a mouse anti-flavivirus protein E antibody (1:1000, MAB10216, Merck-Millipore) and Alexa-488-conjugated goat anti-mouse secondary antibody (1:200, Invitrogen). Cells were analyzed with a Lionheart FX microscope (Biotek, Winooski, VT, USA) with the DAPI filter (Ex 377/50 Em 447/60, Mirror 409), the GFP filter (Ex 469/35 Em 525/39, Mirror 497), and the TRITC filter (Ex 556/20 Em 600/37, Mirror 573). A total of 8 regions of interest were captured per well using the 20X objective, 3-4 wells were analyzed per independent experiment, and four independent experiments were performed. The number of positive cells was determined using the software Gen5 Image Prime 3.03 (Biotek) by automatic and manual detection. The total number of cells in the field was determined by counting the number of nuclei (Hoechst stained); the number of infected cells corresponds to the cells positive to the anti-E antibody; and the percentage of infected cells was obtained by the ratio of nuclei to E-positive cells.

## **ZIKV RNA extraction and quantification**

The viral RNA from culture supernatants obtained at the dpi of interest was used to determine the viral titers. The viral RNA was isolated using the RNA/DNA purification kit

(Magnetic bead) from Da An Gene Co., Ltd. of Sun Yat-Sen University. The absolute quantification was performed using the Prime Script RT-PCR One-Step TB Green II kit (Takara, Bio Inc.) in the 7500 Fast Real-time PCR System (Applied Biosystems). The reaction conditions were 7 minutes at 42°C, 40 cycles of 10 seconds at 95°C, and 1 minute at 60°C, followed by denaturation analysis. The sequences of the primers and the sizes of the amplicon are depicted in Table S1. The RNA levels were quantified using a standard curve with known amounts of ZIKV-ICD plasmid. A total of three independent experiments were performed, and samples were read in duplicate.

## **Determination of metabolic activity and production of reactive oxygen species**

Astrocytes-hNS1 were seeded in 96-well plates at a density of  $1.5 \times 10^4$  cells/well; the next day, they were infected with ZIKV at 0.1 and 1 MOI. At five dpi, the metabolic activity was analyzed using resazurin (Sigma Aldrich) [40, 46], and the production of ROS was determined using 2',7'-dichlorofluorescein diacetate (DCFH-DA, Cat. No D6883, Sigma Aldrich) [47]. Briefly, the medium was removed and replaced with DMEM medium without phenol red and supplemented with resazurin (10 µg/ mL final concentration), then the cells were incubated for 2 hours at 37°C. The metabolic activity was determined by monitoring the fluorescence of resorufin (resazurin metabolized compound) in a Synergy H1 microplate reader (Biotek) at 560 nm excitation and 590 nm emission. For the analysis of ROS production, the medium was replaced with DMEM without phenol red and supplemented with 10 µM DCFH-DA; the cells were incubated for 2 hours at 37°C. The fluorescence reading was performed at 480 nm excitation and 530 nm emission. For both assays, 3 to 4 independent experiments were performed with three experimental replicates, and the fluorescence emitted by uninfected cells was normalized as 100% metabolic activity and ROS production, respectively.

## **Quantification of astrocyte-specific markers and lipid metabolism by RT-qPCR**

Changes in the expression of astrocyte-specific markers and genes involved in hemichannel connection between cells and lipid metabolism were analyzed by RT-qPCR. For this,  $6 \times 10^5$  cells per well were seeded in 6-well plates, infected with ZIKV (MOI of 1), and at five dpi, the total cellular RNA was obtained using Trizol™ (Life Technologies) following the supplier's instructions. Subsequently, 500 ng of cellular RNA were retrotranscribed with the SuperScript II reverse transcription kit (Invitrogen). The relative expression of the genes of interest was determined using a two-step RT-PCR with the iQ SYBR Green Supermix kit (BioRad, Hercules, CA) in the 7500 Fast Real-time PCR System (Applied Biosystems). The setup of the reactions was the following: 95°C for 3 minutes, 40 cycles of 95°C for 10 seconds, and 60°C for 1 minute, followed by thermal denaturation analysis. Primers and amplicons are listed in Table S1. The RNA levels of the genes of interest, as well as of the viral RNA, were normalized using glyceraldehyde-3-phosphate dehydrogenase (GAPDH) expression. The data were analyzed using the  $2^{-\Delta\Delta C_t}$  method. A total of 6 independent experiments were performed.

## **Transmission electron microscopy analysis**

The ultrastructural characterization of infected cells was performed by thin-section TEM. For this,  $6 \times 10^5$  cells per well were seeded in 6-well plates and infected with ZIKV (MOI of 1). The cells were fixed at 3 and 6 dpi with 2% glutaraldehyde, 0.1 M sodium cacodylate, and 0.2% picric acid for 2 hours at room temperature and 72 hours at 4°C. The samples were washed three times with 0.1 M sodium cacodylate pH 7.2, then fixed with 1% osmium tetroxide in 0.1 M sodium cacodylate for 1 hour at room temperature and in the dark, then they were washed twice with the sodium cacodylate buffer, and twice with a 0.1 M sodium

acetate buffer pH 4.5. The cells were stained in block with 0.5% uranyl acetate and 0.1 M sodium acetate for 1 hour at room temperature in the dark, washed three times with 0.1 M sodium acetate, and three times with MilliQ water; then, they were dehydrated with ethanol at increasing concentrations (35%, 50%, 70%, 95%, and 100%) for 10 minutes and three times for each concentration. The cells were washed three times with EMbed 812 resin (Electron Microscopy Sciences). Finally, the resin was allowed to polymerize for 48 hours at 55°C. The polymerized disks were sectioned (70 nm thick sections) using a diamond blade in the LEICA EM UC7 ultramicrotome; the sections were transferred to copper grids and stained with 0.5% uranyl acetate and 0.5% lead citrate in closed Petri dishes containing dry pellets of NaOH. The samples were visualized in the transmission electron microscope JEM- JEOL-2100 at 200 kV, and the images were obtained with the One View Gatan 4K camera. Micrographs were processed in ImageJ software. The number of mitochondria and Lipid Dropets (LDs) per cell were calculated using micrographs at different magnifications and having as reference other cell organelles.

## **Statistical analysis.**

Data were first analyzed to determine their distribution. Data with normal distribution were expressed as mean +/- standard deviation and analyzed with the t-student or ANOVA for multiple comparisons with Bonferroni's posthoc test. Data with non-parametric distribution were expressed as the median and interquartile range (IQR) and analyzed with the U Mann-Whitney or Kruskal-Wallis tests and using Dunn's post hoc test. A  $p < 0.05$  was considered significant. All data were analyzed and graphed using GraphPad software prism 5.0.

# RESULTS

## Generation of astrocytes-hNS1

Astrocytes are a crucial component of the regulation of neurotransmission[48]. They promote myelination, provide support and protection to neurons, and help to maintain the central and peripheral nervous system homeostasis. Astrocytes are the most abundant component of the macroglia in the CNS. To investigate the effects of ZIKV infection on astrocytes we generated cultures of these cells by differentiating the multipotent progenitor hNS-1 cell line (Fig 1). Twenty-one days after the differentiation protocol is started, the progenitor cell line differentiates into two distinct populations: a GFAP-positive population of astrocytes representing  $29.8 \pm 7.6\%$  of the cells in culture, and a neuronal population positive for microtubule-associated protein-2 (MAP-2) representing  $27.2 \pm 7.6\%$  [39, 40]. The other cells in culture remain as undifferentiated hNS-1 cells. Then, the astrocytes are enriched by mechanical and physical exclusion; these cells, unlike hNS-1 and neurons, adhere to culture dishes without poly-L-lysine treatment (Fig 1A). The adherent cells were passed three more times to increase the purity of the culture (Fig 1A). After that, cells were counted by immunofluorescence staining observing that  $93.0 \pm 0.3\%$  were GFAP-positive cells (n=4) (Fig 1B). In addition, the astrocyte cultures were analyzed for expression of the glial cell marker GFAP by end-point PCR, confirming the positivity of this marker (S1 Fig). Finally, we assessed whether the differentiated astrocytes were genomically stable by analyzing the karyotype of different passages (P10, P15, and P22), observing that the chromosomes remained intact (Fig 1C).

## **The Astrocytes-hNS1 are susceptible to Zika virus infection.**

Once the culture of astrocytes-hNS1 was obtained and characterized, we determined whether the cells were susceptible to ZIKV infection (Fig 2). Astrocytes-hNS1 were infected with a MOI of 1, and infection was assessed at three dpi by immunofluorescence staining with an antibody directed against the flavivirus protein E. The average percentage of infected cells was 26% ( $\pm$  4.5%, n=6) (Fig 2A and 2B). RNA was extracted from the culture supernatants of infected cells and the viral load was quantified by RT-qPCR. At 1 dpi the viral production was  $10^{5.9}$  copies/ $\mu$ L, at 2 dpi the production increased to  $10^{6.5}$  copies/ $\mu$ L, and for 3, 4, and 5 dpi the viral production was maintained between  $10^{7.2}$  and  $10^{7.7}$  copies/ $\mu$ L (Fig 2C). In order to determine if there was still viral genome replication at 5 dpi, the cellular RNA was obtained from infected astrocytes and quantified by RT-qPCR. The amount of viral genome in the cell was  $10^{5.8}$  copies/ng of RNA total. Using bright field microscopy, we observed changes in the cell morphology characterized by rounded and refringent cells, accompanied by cells with elongated cell processes, all consistent with a generalized cytopathic effect (see white arrows, Fig 2D). Infection was also confirmed by thin-section TEM of infected cells at 6 dpi, in which we observed the presence of viral particles inside cytoplasmic vesicles (see white arrows, Fig 2E). Altogether these data support that astrocytes-hNS1 are susceptible to ZIKV infection and that at 5 dpi there is still viral genome replication; therefore, they can be a useful model to study the damage that ZIKV causes to cells of the nervous system.

## **Infection affects metabolic activity and production of reactive oxygen species**

We sought to indirectly analyze cell death by measuring changes in the metabolic activity of infected cells through resazurin reduction. The metabolic activity of ZIKV-infected cells at five dpi at MOI of 0.1 and 1 was reduced significantly compared with the uninfected control (set at 100%):  $84.8\% \pm 6.6\%$ ,  $p < 0.05$ , and  $70.3\% \pm 4.8\%$ ,  $p < 0.01$ , respectively (Fig 3A). We evaluated whether the decrease was due to the generation of intracellular ROS using the compound DCFH-DA. Indeed, ROS production was higher in ZIKV-infected astrocytes at five dpi for both, MOI of 0.1 ( $116\% \pm 6.5\%$ ,  $p < 0.05$ ) MOI of 1 ( $122.5\% \pm 5.8\%$ ,  $p < 0.01$ ) (Fig 3B), than in the mock infected cells. These data further confirm that astrocytes-hNS1 can be infected by ZIKV, also arguing that infection decreases cell viability due to a decrease in metabolic activity and an increase in oxidative stress.

## **Infection alters expression of glial proteins**

To analyze whether ZIKV infection compromises the identity and/or function of differentiating/differentiated glial cells, we infected astrocytes-hNS1 at a MOI of 1, and compared the expression of the glial transcripts *GFAP*, *SLC1A3* (encodes EEAT1), *SLC1A2* (encodes EEAT2), *GLUL* (encodes GS), *GRIN1* (encodes N-methyl-D-aspartate Subunit 1 Receptor, *NMDA<sub>R</sub> Subunit 1*) and *GJA1* (encodes connexin-43 (CX43)) at 5 dpi. GFAP is a structural protein that helps to maintain the shape of astrocytes, EAAT1 and EAAT2 are glutamate transporters that internalize glutamate in astrocytes and are thus the main regulators of excitatory glutamate

neurotransmission. GS synthesizes glutamine using glutamate and ammonia as substrates, and with this protects neurons from the toxicity resulting from the excess of these compounds during the events of neuron excitation. NMDAR is an ionotropic glutamate receptor and CX43 is a hemichannel protein found in the gap junctions that connect adjacent cells. [49-51].

We observed that the relative expression of GFAP ( $0.22 \pm 0.04$ ,  $p < 0.001$ ), EAAT1 ( $0.36 \pm 0.07$ ,  $p < 0.001$ ), and GS ( $0.79 \pm 0.11$ ,  $p = 0.06$ ) decreased in infected cells compared with control cells (set to 1) (Fig 4A-C). On the contrary, the relative expression of EAAT2 ( $1.35 \pm 0.3$ ,  $p = 0.06$ ) and Cx43 ( $1.62 \pm 0.7$ ,  $p = 0.1$ ) showed a non-significant trend to increase (Fig 4D and 4E). Finally, the relative expression of the NR1 subunit of NMDAR was significantly upregulated in the infected cells ( $1.78 \pm 0.5$ ,  $p < 0.005$ ) (Fig 4F).

## **Expression of Zika virus entry receptors and genes involved in lipid metabolism**

The TAM (Tyro-3, AXL, and Mertk) family of tyrosine kinase receptors are used for viral entry of flavivirus DENV and ZIKV into host cells [52]. We analyzed the expression of *Tyro-3*, *AXL*, and *Mertk* basally and upon ZIKV infection in our hNS1-derived astrocyte cultures. All three genes were expressed in the absence of infection. However, the expression of *Tyro-3* was reduced upon infection compared with the mock-infected cells (set at 1) ( $0.63 \pm 0.16$ ,  $p = 0.025$ ) (Fig 5A). On the contrary *AXL* and *Mertk* expression increased (*AXL*:  $3.25 \pm 0.54$ ,  $p < 0.001$ ; *Mertk*:  $1.44 \pm 0.21$ ,  $p < 0.05$ ) (Fig 5B and 5C, respectively).



The lipidic component of the cellular membrane also influences flavivirus infection, particularly the amount of cholesterol [53, 54]. We analyzed the expression of the genes encoding the peroxisome proliferator-activated receptor-gamma ( $PPAR-\gamma$ ) and apolipoprotein E ( $APOE$ ) since both are involved in lipid homeostasis. The relative expression of  $PPAR-\gamma$  ( $p=0.39$ ) and  $APOE$  ( $p=0.24$ ) in cells infected with ZIKV (MOI of 1) was not modified (Fig 5D and Fig 5E). These data further support the ability of ZIKV to infect astrocytes-hNS1 through TAM family receptors.

## **Zika virus replication is localized to membranous organelles**

To further understand the infection process of hNS1-derived astrocytes, infected cells were analyzed by thin-section TEM. Fig 6A shows a representative micrograph of an entire astrocyte-hNS1. Cells are characterized by large multilamellar bodies (see blue arrows), which are lipid-rich organelles that contain cytoplasmic material. Fig 6B shows an infected cell at 6 dpi (MOI of 1), in which it can be observed the presence of vacuoles that occupy most of the cytoplasmic space (see red arrows). These vacuoles can be empty or contain smaller vesicles. In Fig 6A we point out to a multilamellar body with blue arrows; however, these structures were very rare in infected cells and were small (see Fig 6B), contrary to uninfected cells. In Figs 6C and D we point out to two different cells with increased levels of viral production. The cell in Fig 6C has only one vesicle that contains viruses (see green arrows); at first glance this is the only modification but as it will be discussed later there is an abnormal mitochondrion, and the rough endoplasmic reticulum (RER) is not visible.

On the contrary, the cell in Fig 6D shows a completely vacuolized cytoplasm, with most of the small vesicles containing viral particles and a RER completely swollen. These two cells may represent different stages of viral infection.

## **Zika virus infection modifies the appearance of mitochondria**

The increase in ROS production suggests possible ZIKV-induced mitochondrial damage. Thus, we further characterize this organelle by thin-section TEM. The morphology of the mitochondria in the mock-infected cells is as expected (*e.g.*, well-defined, and with parallel cristae) (Figs 7A and 7B). However, in ZIKV-infected cells the mitochondria exhibit damage, and this damage seems to depend on the progression of infection. At 3 dpi, mitochondria exhibit concentric cristae, and the external membrane is swollen (Fig 7C). By day 6, mitochondria remain swollen and there is a decrease in the thickness and the number of cristae (Fig 7D). Upon quantification of the number of mitochondria per cell, we did not find significant differences upon infection, 21 and 15 (mock infected day 3 and 6, respectively), 27 (3 dpi) and 21 (6 dpi) (Fig 7E). However, the area of the mitochondria was significantly different, progressively increasing with infection: uninfected cells ( $0.21 \pm 0.15 \mu\text{m}^2$ ), 3 dpi ( $0.34 \pm 0.26 \mu\text{m}^2$ ,  $p < 0.0001$ ) and 6 dpi ( $0.66 \pm 0.38 \mu\text{m}^2$ ,  $p < 0.0001$ ) (Fig 7F). These results strongly suggest mitochondria damage and loss of function upon ZIKV infection.

## Lipid droplets are absent in infected astrocytes

Lipid-droplets (LD) are membraneless organelles that derive from the endoplasmic reticulum and serve to storage lipids [53]. There is evidence that LDs contribute to the assembly of the progeny of some flaviviruses, including DENV and hepatitis C virus [54]. We analyzed LDs in ZIKV-infected astrocytes-hNS1 at 3 and 6 dpi. There were no differences in the morphology of the LD between the mock-infected and infected cells at 3 dpi; however, the electron density of the LD in infected cells seemed lower than in the mock-infected cells (Figs 8A to 8C). Strikingly, by 6 dpi, we could not find LDs in any of the infected cells (Fig 8D). When we quantified the number of LDs, we noticed that there was an increase in the number of LDs at 3 dpi: uninfected cells ( $3.4 \pm 1.2$  LDs/cell) and ZIKV-infected cells ( $28.5 \pm 11.4$  LDs/cell,  $p < 0.001$ ) (Fig 8E). By day 6 pi LDs were absent in infected cells: uninfected cells ( $6.9 \pm 4.3$  LDs/cell) and infected cells (0 LDs/cell,  $p = 0.0058$ ) (Fig 8F). We did not observe changes in the area of the LDs in the infected cells, nor did we observe viral replication associated with these organelles. Altogether we show evidence that astrocytes made from neural progenitor cells are a convenient model to study the damage that ZIKV infection causes in the central nervous system.

## Discussion

ZIKV can infect the developing brain when it crosses the placental and blood-brain barriers. Therefore, ZIKV has been associated with problems in the development of the CNS such as microcephaly, cerebral calcifications, ventriculomegaly, and thin cerebral cortex [8, 11, 12,

53]. In the developing brain, ZIKV can infect NPCs, neurons, and astrocytes. Recent studies have shown that ZIKV infection can persist for at least a month in primary cultures of human astrocytes [28]. Taking this into account, it is plausible that persistently infected astrocytes play an essential role in generating neuronal damage.

In this study, we generated a culture of astrocytes from NPCs. Once we characterized this cell line and determined that it has a correct karyotype and a gene expression profile consistent with glial cells, we decided to analyze the permissibility to ZIKV infection. We show that astrocytes-hNS1s are permissible to ZIKV, and that infection compromises cell survival, measured indirectly through decreased metabolic activity, increased ROS production and gross cytopathic changes, confirming results from another group [27]. We observed about 26% of infected cells at 3 dpi (MOI of 1), which is also similar to a previous study using cultures of human fetal cortical astrocytes infected with clinical isolates of ZIKV [55].

Astrocytes are critical for CNS homeostasis, particularly for the regulation of glutamatergic neurotransmission. We believe that the observation that ZIKV infection decreases *EAAT1* and *GS* expression is relevant and may indicate possible changes in glutamate regulation in the intracellular space. Other viruses also induce neuronal damage by compromising the homeostasis of the glutamatergic system. For instance, human immunodeficiency virus type 1 (HIV-1) infection of fetal cortical astrocytes can decrease the expression of *EAAT1* and *EAAT2* at the messenger and protein levels, and this alters the uptake of <sup>3</sup>H-D-aspartate [56]. The reduced expression of *EAAT1* and *GS* has not been previously reported for ZIKV. Our data call to further investigate whether glutamate uptake is modified and whether this could generate neurons death due to an excess of glutamate.

In a study with isolated rodent cortical neurons, ZIKV infections altered the functionality and expression of NMDA<sub>R</sub> subunits [57]. Olmo et al. found overexpression of NMDA<sub>R</sub> subunit 2 (GLUN2) at 24 hours, accompanied by an increase in the concentration of intracellular calcium and extracellular glutamate. We also found that ZIKV infection increases NMDA<sub>R</sub> expression. Our results open the door to investigate whether there are changes in intracellular calcium due to the activation of NMDA<sub>R</sub> and whether it is accompanied by cell death, as described before [58, 59]. Future studies should also address the expression of other NMDA<sub>R</sub> subunits at the mRNA and protein levels.

We also observed a reduced *GFAP* expression. This data differs from the literature where ZIKV produces glial activation, demonstrated by increased *GFAP* expression [27-29]. However, another study reports a decrease in *GFAP* expression at the protein level when cells are infected with ZIKV [60]. Huang et al (2018) analyzed ZIKV infection in astrocytes and found that many infected cells do not express *GFAP*. They found that infected cells that do not express *GFAP* express *S100-B* (the calcium-binding protein B). The overexpression of *S100-B* demonstrated glial activation [61-63]. It would be interesting to analyze whether the expression of *S100-B* is modified in ZIKV-infected astrocytes-hNS1.

ZIKV, like other flaviviruses, contains phosphatidylserine in the viral envelope, which is taken from the infected cell during viral egress [64]. The incorporation of phosphatidylserine on the viral envelope facilitates viral adsorption and internalization by TAM-mediated phagocytosis. The TAM family of receptors (*e.g.*, Tyro-3, Axl, and Mertk) recognizes the phosphatidylserine present in apoptotic cell membranes, promoting cell phagocytosis. We found that astrocytes-hNS1 expressed all three genes, perhaps explaining their permissibility to ZIKV infection. The gene expression of TAM receptors is modified at five dpi. On the one hand, AXL and Mertk are overexpressed. Ojha and collaborators analyzed the expression of TAM receptors in primary cultures of astrocytes. They found that AXL was overexpressed, and that

blockade of this receptor decreased viral infection [29]. The expression of AXL in astrocytes-hNS1 is consistent with reports showing that infection in astrocytes is mediated by AXL [26, 29]. On the other hands, we found that ZIKV infection decreases tyro-3 expression. The expression of tyro-3 is consistent with a study in placentas, where Tyro-3 expression was decreased [65]. However, other studies have shown that Tyro-3 is increased in astrocytes [29]. These discrepancies could be due to multiple factors, among the most important, the viral strains, the number of passages to obtain the virus, the origin of astrocytes, the purity of the culture, the MOI used and the time of infection.

The PPAR $\gamma$  gene is a regulator of lipid metabolism that participates in adipogenesis [66]. Different cellular factors necessary for flavivirus replication are involved in the metabolism of lipids [54, 67]. We did not see changes in the expression of PPAR $\gamma$  after infection. Overexpression of PPAR $\gamma$  has been previously reported in NPCs infected with ZIKV [32, 66].

The apolipoprotein E (APOE) is a highly expressed protein with a central role in lipid metabolism in neural cells [68, 69], so we were interested in knowing if there was a relationship between APOE expression and ZIKV production in astrocytes. We report that there are no changes at the transcriptional level of this gene. Our thin-section TEM data clearly shows that upon infection there is an alteration of the lipid metabolism; we observed a decrease in the number of large multilamellar bodies, and an increase followed by a decrease in the number of LD. Therefore, in our culture of astrocytes, other genes must be participating in regulating the metabolism distribution of lipids that help the production of ZIKV viral particles.

Finally, we demonstrate, by thin-section TEM, how ZIKV infection structurally modifies hNS1-derived astrocytes. The first approach we carried out was to analyze the changes in the mitochondria, finding that the number of mitochondria per cell was maintained in ZIKV-

infected and uninfected cells. However, when analyzing the size of the mitochondria (mitochondrial area,  $\mu\text{m}^2$ ), we found that the mitochondrial area greater in infected cells at both three and six dpi than in the controls. We also found that the integrity of the cristae and their organization is affected by the infection. This could suggest a possible mitophagy process, which has been previously observed in ZIKV [70] and classical swine fever virus (CSFV) [71]. Mitochondria play a fundamental role in the energy supply for the cell. In the infected condition, the mitochondria will be overloaded, as the energy requirements for cell survival and virion production imply energy use. An increase in ROS can be presented by mitochondrial overload. Damage to mitochondria has been analyzed in various studies. For example, by using astrocytes derived from NPCs and infecting them with ZIKV, it was shown that the infection could increase ATP synthesis at 18 hpi, but the ATP reserve capacity is reduced to 24, 36, and 48 hpi. Furthermore, at 48 hpi, a decrease in mitochondrial respiration routine is observed due to mitochondrial damage produced by ROS [27]. In another study, using ZIKV-infected human retinal epithelial cells, a change in mitochondrial morphology was observed by confocal microscopy and changes in mitochondrial membrane potential, suggesting that ZIKV infection induces an imbalance of fusion/fission of mitochondria [72].

Interestingly, at three dpi the number of LDs per cell was higher in ZIKV-infected than in the mock-infected cells. However, when looking at cells at six dpi, LDs were absent in infected cells. The area of the LDs was similar in both infected and uninfected cells at three dpi and in uninfected cells at six dpi. The dynamics with which these cellular compartments appear to increase and ultimately decrease tell us about lipids influence on the ZIKV viral cycle. Garcia et al. (2020) used Huh-7 cells to characterize changes in LDs at 24 hpi and found that the number of LDs/cell was higher in uninfected cells compared to ZIKV-infected cells. Furthermore, a decreased volume of LDs was observed in ZIKV-infected cells compared to uninfected cells [72]. We believe that the decrease in LDs in astrocytes occurs due to the

production of viral particles since the replication of some flaviviruses, for example, DENV, depends on the  $\beta$ -oxidation of triglycerides present in LDs [73, 74]. The use of lipid droplets as lipid substrates could explain why in our work, the amount of LD decreases at higher times of infection (6 dpi), which coincides in being the post-infection time in which more viral particles and a lower amount of LD.

Research on cellular factors necessary for viral replication, such as lipids, offers information for the development of treatments that could prevent the generation of microcephaly and other malformations associated with ZIKV infection in pregnancy. Given the great importance of lipids in the viral production cycle, it could look at the potential of agents that inhibit lipid biosynthesis and have been shown not to interfere with pregnancy, for example, metformin [54].

In summary, we developed a culture of astrocytes that were derived and purified from pluripotent cells. The astrocytes-hNS1 were characterized by analyzing the expression of the GFAP marker and the gene expression of GFAP, EAAT1, EAAT2, and GS. This culture maintained a stable karyotype. Furthermore, astrocytes-hNS1 are susceptible and permissive to ZIKV infection. This viral infection leads to ROS production and a decrease in cell viability, the gene expression for GFAP, EAAT1, and GS is downregulated while for NMDA<sub>R</sub> increased. This suggests that there are changes that compromise the homeostasis of neuronal communication, specifically communication by glutamatergic neurotransmission. The overexpression of Mertk and AXL, and the downregulation of Tyro-3 suggest that these are receptors that promote ZIKV infection in our culture. Finally, we found changes in the size of the mitochondria and a decrease in the number of LDs in the cells, which helps us better understand virion production and propose experiments that help develop therapies to mitigate the effects of ZIKV infection.



The data presented here show the overall effect of ZIKV in infected cells; however, in order to determine if changes in cell morphology and biochemistry are the result of an early inflammatory process or a consequence of the cytopathic effects, we would like to perform blocking experiments that help us to separate the effects of these processes. However, blocking ZIKV entry is a complex experimental problem. There are multiple candidate receptors involved in ZIKV infection [75]. In cells of the nervous system the expression of at least four proteins has been associated with ZIKV entry: DC-SIGN [76], Tyro-3 [77], AXL [26, 78], and Mertk [77]. Although carrying out the blocking experiments of these receptors would represent a greater understanding of the mechanism underlying the viral infection, these methodological approaches are beyond the scope of our work, so it could be a perspective for addressing in the future. As it has been shown by others [26, 65, 75, 78] blocking one receptor at a time is not enough to completely block entry; hence, in order to completely inhibit viral entry, we would have to block the interaction of the virus with multiple receptors. Furthermore, given the role of these proteins in the biology of neural cells it is possible that blocking these receptors could result in profound cellular alterations that could hamper our understanding of the effects of the viral infection on these cells.

Although the question remains whether ZIKV will ever be able to cross the adult blood-brain barrier and affect the brain, astrocytes are highly susceptible to ZIKV, posing a high risk, especially for pregnant women. Astrocytes control redox homeostasis, help control neuronal communication, and maintain the blood-brain barrier in optimal conditions. A decrease in the number of astrocytes can lead to motor and cognitive problems and neuronal loss without the need for ZIKV to infect neuronal cells. Therefore, it would be worth studying the infection of this type of cells in depth to generate drug therapies in the future.

## Acknowledgments

EI.R.H (CVU: 775486) and M.C.S. (CVU: 714882) received scholarships from CONACYT.

M. Sc Arleth Miranda Lopez for her advice on the karyotype technique.

Dr. Fernando Peña Ortega, Dra. Adriana Monsiváis Urenda, and Dr. Christian García Sepulveda by suggestions during the PhD of EI.R.H.

Dr. Alberto Martínez-Serrano ("Severo Ochoa" Molecular Biology Center, Madrid, Spain) for donating the hNS-1 cell line.

Dr. Ezequiel Fuentes Pananá by suggestions and revision of original paper.

## References

1. White MK, Wollebo HS, David Beckham J, Tyler KL, Khalili K. Zika virus: An emergent neuropathological agent. *Ann Neurol*. 2016;80(4):479-89. Epub 08/10. doi: 10.1002/ana.24748. PubMed PMID: 27464346.
2. Wikan N, Smith DR. Zika virus: history of a newly emerging arbovirus. *The Lancet Infectious Diseases*. 2016;16(7):e119-e26. doi: [https://doi.org/10.1016/S1473-3099\(16\)30010-X](https://doi.org/10.1016/S1473-3099(16)30010-X).
3. Dick GW, Kitchen SF, Haddow AJ. Zika virus. I. Isolations and serological specificity. *Transactions of the Royal Society of Tropical Medicine and Hygiene*. 1952;46(5):509-20. Epub 1952/09/01. doi: 10.1016/0035-9203(52)90042-4. PubMed PMID: 12995440.
4. Gorshkov K, Shiryaev SA, Fertel S, Lin YW, Huang CT, Pinto A, et al. Zika Virus: Origins, Pathological Action, and Treatment Strategies. *Frontiers in microbiology*. 2018;9:3252. Epub 2019/01/23. doi: 10.3389/fmicb.2018.03252. PubMed PMID: 30666246; PubMed Central PMCID: PMC6330993.

5. Sheridan MA, Balaraman V, Schust DJ, Ezashi T, Roberts RM, Franz AWE. African and Asian strains of Zika virus differ in their ability to infect and lyse primitive human placental trophoblast. *PloS one*. 2018;13(7):e0200086. Epub 2018/07/10. doi: 10.1371/journal.pone.0200086. PubMed PMID: 29985932; PubMed Central PMCID: PMC6037361 Board member. This does not alter the authors' adherence to PLOS ONE Editorial policies and criteria.
6. Nunes BTD, Fontes-Garfias CR, Shan C, Muruato AE, Nunes JGC, Burbano RMR, et al. Zika structural genes determine the virulence of African and Asian lineages. *Emerging microbes & infections*. 2020;9(1):1023-33. Epub 2020/05/19. doi: 10.1080/22221751.2020.1753583. PubMed PMID: 32419649; PubMed Central PMCID: PMC68284969.
7. Krow-Lucal ER, de Andrade MR, Cananéa JNA, Moore CA, Leite PL, Biggerstaff BJ, et al. Association and birth prevalence of microcephaly attributable to Zika virus infection among infants in Paraíba, Brazil, in 2015-2016: a case-control study. *The Lancet Child & Adolescent Health*. 2018;2(3):205-13. doi: 10.1016/S2352-4642(18)30020-8.
8. Oliveira-Szejnfeld PSd, Levine D, Melo ASdO, Amorim MMR, Batista AGM, Chimelli L, et al. Congenital Brain Abnormalities and Zika Virus: What the Radiologist Can Expect to See Prenatally and Postnatally. *Radiology*. 2016;281(1):203-18. doi: 10.1148/radiol.2016161584. PubMed PMID: 27552432.
9. Li H, Saucedo-Cuevas L, Shresta S, Gleeson JG. The Neurobiology of Zika Virus. *Neuron*. 2016;92(5):949-58. Epub 2016/12/09. doi: 10.1016/j.neuron.2016.11.031. PubMed PMID: 27930910.
10. Mittal S, Federman HG, Sievert D, Gleeson JG. The Neurobiology of Modern Viral Scourges: ZIKV and COVID-19. *The Neuroscientist : a review journal bringing neurobiology, neurology and psychiatry*. 2021:10738584211009149. Epub 2021/04/21. doi: 10.1177/10738584211009149. PubMed PMID: 33874789.
11. Zhang ZW, Li ZL, Yuan S. The Role of Secretory Autophagy in Zika Virus Transfer through the Placental Barrier. *Frontiers in cellular and infection*

microbiology. 2016;6:206. Epub 2017/01/26. doi: 10.3389/fcimb.2016.00206. PubMed PMID: 28119857; PubMed Central PMCID: PMC5220013.

12. Chiu CF, Chu LW, Liao IC, Simanjuntak Y, Lin YL, Juan CC, et al. The Mechanism of the Zika Virus Crossing the Placental Barrier and the Blood-Brain Barrier. *Frontiers in microbiology*. 2020;11:214. Epub 2020/03/11. doi: 10.3389/fmicb.2020.00214. PubMed PMID: 32153526; PubMed Central PMCID: PMC7044130.

13. Ferraris P, Cochet M, Hamel R, Gladwyn-Ng I, Alfano C, Diop F, et al. Zika virus differentially infects human neural progenitor cells according to their state of differentiation and dysregulates neurogenesis through the Notch pathway. *Emerging microbes & infections*. 2019;8(1):1003-16. Epub 2019/07/10. doi: 10.1080/22221751.2019.1637283. PubMed PMID: 31282298; PubMed Central PMCID: PMC6691766.

14. Gabriel E, Ramani A, Karow U, Gottardo M, Natarajan K, Gooi LM, et al. Recent Zika Virus Isolates Induce Premature Differentiation of Neural Progenitors in Human Brain Organoids. *Cell stem cell*. 2017;20(3):397-406.e5. Epub 2017/01/31. doi: 10.1016/j.stem.2016.12.005. PubMed PMID: 28132835.

15. Ghezzi S, Cooper L, Rubio A, Pagani I, Capobianchi MR, Ippolito G, et al. Heparin prevents Zika virus induced-cytopathic effects in human neural progenitor cells. *Antiviral research*. 2017;140:13-7. Epub 2017/01/09. doi: 10.1016/j.antiviral.2016.12.023. PubMed PMID: 28063994; PubMed Central PMCID: PMC7113768.

16. Lee JK, Kim JA, Oh SJ, Lee EW, Shin OS. Zika Virus Induces Tumor Necrosis Factor-Related Apoptosis Inducing Ligand (TRAIL)-Mediated Apoptosis in Human Neural Progenitor Cells. *Cells*. 2020;9(11). Epub 2020/11/20. doi: 10.3390/cells9112487. PubMed PMID: 33207682; PubMed Central PMCID: PMC7697661.

17. Rychlowska M, Agyapong A, Weinfeld M, Schang LM. Zika Virus Induces Mitotic Catastrophe in Human Neural Progenitors by Triggering Unscheduled Mitotic

Entry in the Presence of DNA Damage While Functionally Depleting Nuclear PNKP. *Journal of virology*. 2022;96(9):e0033322. Epub 2022/04/13. doi: 10.1128/jvi.00333-22. PubMed PMID: 35412344; PubMed Central PMCID: PMC9093132.

18. Thulasi Raman SN, Latreille E, Gao J, Zhang W, Wu J, Russell MS, et al. Dysregulation of Ephrin receptor and PPAR signaling pathways in neural progenitor cells infected by Zika virus. *Emerging microbes & infections*. 2020;9(1):2046-60. doi: 10.1080/22221751.2020.1818631. PubMed PMID: 32873194.

19. Xu YP, Qiu Y, Zhang B, Chen G, Chen Q, Wang M, et al. Zika virus infection induces RNAi-mediated antiviral immunity in human neural progenitors and brain organoids. 2019;29(4):265-73. doi: 10.1038/s41422-019-0152-9. PubMed PMID: 30814679.

20. Garcez PP, Loiola EC, Madeiro da Costa R, Higa LM, Trindade P, Delvecchio R, et al. Zika virus impairs growth in human neurospheres and brain organoids. *Science*. 2016;352(6287):816-8. doi: doi:10.1126/science.aaf6116.

21. Qian X, Nguyen HN, Song MM, Hadiono C, Ogden SC, Hammack C, et al. Brain-Region-Specific Organoids Using Mini-bioreactors for Modeling ZIKV Exposure. *Cell*. 2016;165(5):1238-54. Epub 2016/04/28. doi: 10.1016/j.cell.2016.04.032. PubMed PMID: 27118425; PubMed Central PMCID: PMC4900885.

22. Braz-De-Melo HA, Pasquarelli-do-Nascimento G, Corrêa R, das Neves Almeida R, de Oliveira Santos I, Prado PS, et al. Potential neuroprotective and anti-inflammatory effects provided by omega-3 (DHA) against Zika virus infection in human SH-SY5Y cells. 2019;9(1):20119. doi: 10.1038/s41598-019-56556-y. PubMed PMID: 31882804.

23. Bonenfant G, Meng R, Shotwell C. Asian Zika Virus Isolate Significantly Changes the Transcriptional Profile and Alternative RNA Splicing Events in a Neuroblastoma Cell Line. 2020;12(5). doi: 10.3390/v12050510. PubMed PMID: 32380717.

24. Gaburro J, Bhatti A, Sundaramoorthy V, Dearnley M, Green D, Nahavandi S, et al. Zika virus-induced hyper excitation precedes death of mouse primary neuron. 2018;15(1):79. doi: 10.1186/s12985-018-0989-4. PubMed PMID: 29703263.
25. Schultz V, Cumberworth SL, Gu Q, Johnson N. Zika Virus Infection Leads to Demyelination and Axonal Injury in Mature CNS Cultures. 2021;13(1). doi: 10.3390/v13010091. PubMed PMID: 33440758.
26. Chen J, Yang Y-f, Yang Y, Zou P, Chen J, He Y, et al. AXL promotes Zika virus infection in astrocytes by antagonizing type I interferon signalling. Nature Microbiology. 2018;3(3):302-9. doi: 10.1038/s41564-017-0092-4.
27. Ledur PF, Karmirian K, Pedrosa C, Souza LRQ, Assis-de-Lemos G, Martins TM, et al. Zika virus infection leads to mitochondrial failure, oxidative stress and DNA damage in human iPSC-derived astrocytes. Scientific reports. 2020;10(1):1218. Epub 2020/01/29. doi: 10.1038/s41598-020-57914-x. PubMed PMID: 31988337; PubMed Central PMCID: PMC6985105.
28. Limonta D, Jovel J, Kumar A, Airo AM, Hou S, Saito L, et al. Human Fetal Astrocytes Infected with Zika Virus Exhibit Delayed Apoptosis and Resistance to Interferon: Implications for Persistence. Viruses. 2018;10(11). Epub 2018/11/21. doi: 10.3390/v10110646. PubMed PMID: 30453621; PubMed Central PMCID: PMC6266559.
29. Ojha CR, Rodriguez M, Karuppan MKM, Lapierre J, Kashanchi F, El-Hage N. Toll-like receptor 3 regulates Zika virus infection and associated host inflammatory response in primary human astrocytes. PloS one. 2019;14(2):e0208543-e. doi: 10.1371/journal.pone.0208543. PubMed PMID: 30735502.
30. Wen C, Yu Y, Gao C, Qi X, Cardona CJ, Xing Z. RIPK3-Dependent Necroptosis Is Induced and Restricts Viral Replication in Human Astrocytes Infected With Zika Virus. Frontiers in cellular and infection microbiology. 2021;11:637710. Epub 2021/04/03. doi: 10.3389/fcimb.2021.637710. PubMed PMID: 33796483; PubMed Central PMCID: PMC8007970.

31. Tang H, Hammack C, Ogden SC, Wen Z, Qian X, Li Y, et al. Zika Virus Infects Human Cortical Neural Progenitors and Attenuates Their Growth. *Cell stem cell*. 2016;18(5):587-90. Epub 2016/03/10. doi: 10.1016/j.stem.2016.02.016. PubMed PMID: 26952870; PubMed Central PMCID: PMC5299540.
32. Li H, Saucedo-Cuevas L, Regla-Nava JA, Chai G, Sheets N, Tang W, et al. Zika Virus Infects Neural Progenitors in the Adult Mouse Brain and Alters Proliferation. *Cell stem cell*. 2016;19(5):593-8. Epub 2016/08/23. doi: 10.1016/j.stem.2016.08.005. PubMed PMID: 27545505; PubMed Central PMCID: PMC5097023.
33. Goodfellow FT, Willard KA, Wu X, Scoville S, Stice SL, Brindley MA. Strain-Dependent Consequences of Zika Virus Infection and Differential Impact on Neural Development. *Viruses*. 2018;10(10). Epub 2018/10/12. doi: 10.3390/v10100550. PubMed PMID: 30304805; PubMed Central PMCID: PMC6212967.
34. Depla JA, Mulder LA, de Sá RV, Wartel M, Sridhar A, Evers MM, et al. Human Brain Organoids as Models for Central Nervous System Viral Infection. *Viruses*. 2022;14(3). Epub 2022/03/27. doi: 10.3390/v14030634. PubMed PMID: 35337041; PubMed Central PMCID: PMC8948955.
35. Galland F, Seady M, Taday J, Smaili SS, Gonçalves CA, Leite MC. Astrocyte culture models: Molecular and function characterization of primary culture, immortalized astrocytes and C6 glioma cells. *Neurochemistry International*. 2019;131:104538. doi: <https://doi.org/10.1016/j.neuint.2019.104538>.
36. Verkhratsky A, Nedergaard M, Hertz L. Why are astrocytes important? *Neurochemical research*. 2015;40(2):389-401. Epub 2014/08/13. doi: 10.1007/s11064-014-1403-2. PubMed PMID: 25113122.
37. Kozak RA, Majer A, Biondi MJ, Medina SJ, Goneau LW, Sajesh BV, et al. MicroRNA and mRNA Dysregulation in Astrocytes Infected with Zika Virus. *Viruses*. 2017;9(10). Epub 2017/10/19. doi: 10.3390/v9100297. PubMed PMID: 29036922; PubMed Central PMCID: PMC5691648.

38. Villa A, Snyder EY, Vescovi A, Martínez-Serrano A. Establishment and Properties of a Growth Factor-Dependent, Perpetual Neural Stem Cell Line from the Human CNS. *Experimental Neurology*. 2000;161(1):67-84. doi: <https://doi.org/10.1006/exnr.1999.7237>.
39. Villa A, Navarro-Galve B, Bueno C, Franco S, Blasco MA, Martinez-Serrano A. Long-term molecular and cellular stability of human neural stem cell lines. *Experimental cell research*. 2004;294(2):559-70. Epub 2004/03/17. doi: 10.1016/j.yexcr.2003.11.025. PubMed PMID: 15023542.
40. González-Sánchez HM, Monsiváis-Urenda A, Salazar-Aldrete CA, Hernández-Salinas A, Noyola DE, Jiménez-Capdeville ME, et al. Effects of cytomegalovirus infection in human neural precursor cells depend on their differentiation state. *Journal of neurovirology*. 2015;21(4):346-57. Epub 2015/04/09. doi: 10.1007/s13365-015-0315-5. PubMed PMID: 25851778.
41. Zheng J, Ghorpade A, Niemann D, Cotter RL, Thylin MR, Epstein L, et al. Lymphotropic virions affect chemokine receptor-mediated neural signaling and apoptosis: implications for human immunodeficiency virus type 1-associated dementia. *Journal of virology*. 1999;73(10):8256-67. doi: 10.1128/JVI.73.10.8256-8267.1999. PubMed PMID: 10482576.
42. Canki M, Thai JN, Chao W, Ghorpade A, Potash MJ, Volsky DJ. Highly productive infection with pseudotyped human immunodeficiency virus type 1 (HIV-1) indicates no intracellular restrictions to HIV-1 replication in primary human astrocytes. *Journal of virology*. 2001;75(17):7925-33. doi: 10.1128/jvi.75.17.7925-7933.2001. PubMed PMID: 11483737.
43. Bernabeu-Zornoza A, Coronel R, Palmer C, Calero M, Martínez-Serrano A, Cano E, et al. A $\beta$ 42 Peptide Promotes Proliferation and Gliogenesis in Human Neural Stem Cells. *Molecular Neurobiology*. 2019;56(6):4023-36. doi: 10.1007/s12035-018-1355-7.
44. Tsetsarkin KA, Kenney H, Chen R, Liu G, Manukyan H, Whitehead SS, et al. A Full-Length Infectious cDNA Clone of Zika Virus from the 2015 Epidemic in Brazil



as a Genetic Platform for Studies of Virus-Host Interactions and Vaccine Development. *mBio*. 2016;7(4). Epub 2016/08/25. doi: 10.1128/mBio.01114-16. PubMed PMID: 27555311; PubMed Central PMCID: PMC4999549.

45. Guo L, Wang L, Yang R, Feng R, Li Z, Zhou X, et al. Optimizing conditions for calcium phosphate mediated transient transfection. *Saudi J Biol Sci*. 2017;24(3):622-9. Epub 02/11. doi: 10.1016/j.sjbs.2017.01.034. PubMed PMID: 28386188.

46. Castillo C, Rubio EI, Santos H, Paredes A. Cultivo de Células Progenitoras Neurales Humanas sobre Andamios de Ácido Poli-Láctico (PLA) Generados por Impresión 3D para su Aplicación en Lesiones Medulares. *Memorias del Congreso Nacional de Ingeniería Biomédica*. 2017;3(1):152-6.

47. Silva-Ramirez AS, Castillo CG, Navarro-Tovar G, Gonzalez-Sanchez HM, Rocha-Uribe A, Gonzalez-Chavez MM, et al. Bioactive Isomers of Conjugated Linoleic Acid Inhibit the Survival of Malignant Glioblastoma Cells But Not Primary Astrocytes. *European Journal of Lipid Science and Technology*. 2018;120(11):1700454. doi: <https://doi.org/10.1002/ejlt.201700454>.

48. Schousboe A. Metabolic signaling in the brain and the role of astrocytes in control of glutamate and GABA neurotransmission. *Neuroscience letters*. 2019;689:11-3. Epub 2018/01/30. doi: 10.1016/j.neulet.2018.01.038. PubMed PMID: 29378296.

49. Lee MC, Ting KK, Adams S, Brew BJ, Chung R, Guillemin GJ. Characterisation of the expression of NMDA receptors in human astrocytes. *PloS one*. 2010;5(11):e14123. Epub 2010/12/15. doi: 10.1371/journal.pone.0014123. PubMed PMID: 21152063; PubMed Central PMCID: PMC2994931.

50. Verkhratsky A, Kirchhoff F. NMDA Receptors in glia. *The Neuroscientist : a review journal bringing neurobiology, neurology and psychiatry*. 2007;13(1):28-37. Epub 2007/01/19. doi: 10.1177/1073858406294270. PubMed PMID: 17229973.

51. Verkhratsky A, Chvátal A. NMDA Receptors in Astrocytes. *Neurochemical research*. 2020;45(1):122-33. Epub 2019/02/16. doi: 10.1007/s11064-019-02750-3. PubMed PMID: 30767094.
52. Ghosh Roy S. TAM receptors: A phosphatidylserine receptor family and its implications in viral infections. *International review of cell and molecular biology*. 2020;357:81-122. Epub 2020/11/26. doi: 10.1016/bs.ircmb.2020.09.003. PubMed PMID: 33234246.
53. Chen Q, Gouilly J, Ferrat YJ, Espino A, Glaziou Q, Cartron G, et al. Metabolic reprogramming by Zika virus provokes inflammation in human placenta. *Nat Commun*. 2020;11(1):2967-. doi: 10.1038/s41467-020-16754-z. PubMed PMID: 32528049.
54. Farfan-Morales CN, Cordero-Rivera CD, Reyes-Ruiz JM, Hurtado-Monzón AM, Osuna-Ramos JF, González-González AM, et al. Anti-flavivirus Properties of Lipid-Lowering Drugs. *Front Physiol*. 2021;12:749770-. doi: 10.3389/fphys.2021.749770. PubMed PMID: 34690817.
55. Jorgačevski J, Korva M, Potokar M, Lisjak M, Avšič-Županc T, Zorec R. ZIKV Strains Differentially Affect Survival of Human Fetal Astrocytes versus Neurons and Traffic of ZIKV-Laden Endocytotic Compartments. *Scientific reports*. 2019;9(1):8069. Epub 2019/05/31. doi: 10.1038/s41598-019-44559-8. PubMed PMID: 31147629; PubMed Central PMCID: PMCPMC6542792.
56. Moidunny S, Matos M, Wesseling E, Banerjee S, Volsky DJ, Cunha RA, et al. Oncostatin M promotes excitotoxicity by inhibiting glutamate uptake in astrocytes: implications in HIV-associated neurotoxicity. *Journal of Neuroinflammation*. 2016;13(1):144. doi: 10.1186/s12974-016-0613-8.
57. Olmo IG, Carvalho TG, Costa VV, Alves-Silva J, Ferrari CZ, Izidoro-Toledo TC, et al. Zika Virus Promotes Neuronal Cell Death in a Non-Cell Autonomous Manner by Triggering the Release of Neurotoxic Factors. *Frontiers in immunology*. 2017;8:1016. Epub 2017/09/08. doi: 10.3389/fimmu.2017.01016. PubMed PMID: 28878777; PubMed Central PMCID: PMCPMC5572413.

58. de Vera N, Martínez E, Sanfeliu C. Spermine induces cell death in cultured human embryonic cerebral cortical neurons through N-methyl-D-aspartate receptor activation. *Journal of Neuroscience Research*. 2008;86(4):861-72. doi: <https://doi.org/10.1002/jnr.21538>.
59. Reyes RC, Brennan AM, Shen Y, Baldwin Y, Swanson RA. Activation of neuronal NMDA receptors induces superoxide-mediated oxidative stress in neighboring neurons and astrocytes. *The Journal of neuroscience : the official journal of the Society for Neuroscience*. 2012;32(37):12973-8. Epub 2012/09/14. doi: 10.1523/jneurosci.1597-12.2012. PubMed PMID: 22973021; PubMed Central PMCID: PMCPmc3478885.
60. Huang Y, Li Y, Zhang H, Zhao R, Jing R, Xu Y, et al. Zika virus propagation and release in human fetal astrocytes can be suppressed by neutral sphingomyelinase-2 inhibitor GW4869. *Cell discovery*. 2018;4:19. Epub 2018/05/01. doi: 10.1038/s41421-018-0017-2. PubMed PMID: 29707233; PubMed Central PMCID: PMCPMC5913238.
61. da Cunha Franceschi R, Nardin P, Machado CV, Tortorelli LS, Martinez-Pereira MA, Zanotto C, et al. Enteric glial reactivity to systemic LPS administration: Changes in GFAP and S100B protein. *Neuroscience research*. 2017;119:15-23. Epub 2017/01/09. doi: 10.1016/j.neures.2016.12.005. PubMed PMID: 28063977.
62. Ding S, Wang C, Wang W, Yu H, Chen B, Liu L, et al. Autocrine S100B in astrocytes promotes VEGF-dependent inflammation and oxidative stress and causes impaired neuroprotection. *Cell biology and toxicology*. 2021. Epub 2021/11/19. doi: 10.1007/s10565-021-09674-1. PubMed PMID: 34792689.
63. Galland F, Seady M, Taday J, Smaili SS, Gonçalves CA, Leite MC. Astrocyte culture models: Molecular and function characterization of primary culture, immortalized astrocytes and C6 glioma cells. *Neurochemistry international*. 2019;131:104538. Epub 2019/08/21. doi: 10.1016/j.neuint.2019.104538. PubMed PMID: 31430518.

64. Perera-Lecoin M, Meertens L, Carnec X, Amara A. Flavivirus entry receptors: an update. *Viruses*. 2013;6(1):69-88. Epub 2014/01/02. doi: 10.3390/v6010069. PubMed PMID: 24381034; PubMed Central PMCID: PMC3917432.
65. Nobrega GM, Samogim AP, Parise PL, Venceslau EM, Guida JPS, Japacanga RR, et al. TAM and TIM receptors mRNA expression in Zika virus infected placentas. *Placenta*. 2020;101:204-7. doi: <https://doi.org/10.1016/j.placenta.2020.09.062>.
66. Layrolle P, Payoux P, Chavanas S. PPAR Gamma and Viral Infections of the Brain. *International journal of molecular sciences*. 2021;22(16). Epub 2021/08/28. doi: 10.3390/ijms22168876. PubMed PMID: 34445581; PubMed Central PMCID: PMC8396218.
67. Ci Y, Shi L. Compartmentalized replication organelle of flavivirus at the ER and the factors involved. *Cellular and molecular life sciences : CMLS*. 2021;78(11):4939-54. Epub 2021/04/14. doi: 10.1007/s00018-021-03834-6. PubMed PMID: 33846827; PubMed Central PMCID: PMC8041242.
68. Huang Y, Mahley RW. Apolipoprotein E: structure and function in lipid metabolism, neurobiology, and Alzheimer's diseases. *Neurobiology of disease*. 2014;72 Pt A:3-12. Epub 2014/09/01. doi: 10.1016/j.nbd.2014.08.025. PubMed PMID: 25173806; PubMed Central PMCID: PMC4253862.
69. Gong Y, Cun W. The Role of ApoE in HCV Infection and Comorbidity. *International journal of molecular sciences*. 2019;20(8). Epub 2019/04/28. doi: 10.3390/ijms20082037. PubMed PMID: 31027190; PubMed Central PMCID: PMC6515466.
70. Ponia SS, Robertson SJ, McNally KL, Subramanian G, Sturdevant GL, Lewis M, et al. Mitophagy antagonism by ZIKV reveals Ajuba as a regulator of PINK1 signaling, PKR-dependent inflammation, and viral invasion of tissues. *Cell Reports*. 2021;37(4). doi: 10.1016/j.celrep.2021.109888. PubMed PMID: 109888.
71. Gou H, Zhao M, Xu H, Yuan J, He W, Zhu M, et al. CSFV induced mitochondrial fission and mitophagy to inhibit apoptosis. *Oncotarget*.

2017;8(24):39382-400. Epub 2017/04/30. doi: 10.18632/oncotarget.17030. PubMed PMID: 28455958; PubMed Central PMCID: PMCPmc5503620.

72. García CC, Vázquez CA, Giovannoni F, Russo CA, Cordo SM, Alaimo A, et al. Cellular Organelles Reorganization During Zika Virus Infection of Human Cells. *Frontiers in microbiology*. 2020;11.

73. Heaton NS, Randall G. Dengue virus-induced autophagy regulates lipid metabolism. *Cell host & microbe*. 2010;8(5):422-32. Epub 2010/11/16. doi: 10.1016/j.chom.2010.10.006. PubMed PMID: 21075353; PubMed Central PMCID: PMCPmc3026642.

74. Zhang J, Lan Y, Sanyal S. Modulation of Lipid Droplet Metabolism-A Potential Target for Therapeutic Intervention in Flaviviridae Infections. *Frontiers in microbiology*. 2017;8:2286. Epub 2017/12/14. doi: 10.3389/fmicb.2017.02286. PubMed PMID: 29234310; PubMed Central PMCID: PMCPmc5712332.

75. Agrelli A, de Moura RR, Crovella S, Brandão LAC. ZIKA virus entry mechanisms in human cells. *Infection, Genetics and Evolution*. 2019;69:22-9. doi: <https://doi.org/10.1016/j.meegid.2019.01.018>.

76. Deiva K, Khiati A, Hery C, Salim H, Leclerc P, Horellou P, et al. CCR5-, DC-SIGN-dependent endocytosis and delayed reverse transcription after human immunodeficiency virus type 1 infection in human astrocytes. *AIDS research and human retroviruses*. 2006;22(11):1152-61. Epub 2006/12/07. doi: 10.1089/aid.2006.22.1152. PubMed PMID: 17147503.

77. Ji R, Meng L, Jiang X, Cvm NK, Ding J, Li Q, et al. TAM Receptors Support Neural Stem Cell Survival, Proliferation and Neuronal Differentiation. *PLoS one*. 2014;9(12):e115140. doi: 10.1371/journal.pone.0115140.

78. Jimenez OA, Narasipura SD, Barbian HJ, Albalawi YA, Seaton MS, Robinson KF, et al.  $\beta$ -Catenin Restricts Zika Virus Internalization by Downregulating Axl. *Journal of virology*. 2021;95(17):e0070521. Epub 2021/07/15. doi: 10.1128/jvi.00705-21. PubMed PMID: 34260264; PubMed Central PMCID: PMCPMC8354222.

## Figure legends:

**Fig 1. Astrocytes-hNS1 are a pure culture of human astrocytes.** hNS-1 cells were differentiated for 21 days. The differentiated cells were harvested and seeded in culture labware without poly-L-lysine treatment and with DMEM. Non-adherent cells (neurons and neural progenitor cells that did not differentiate) were removed by exchanging the media. Astrocytes-hNS1 cells were seeded, and cells were fixed and processed for immunofluorescence using antibodies to GFAP (astrocyte marker). Cells from different passages were used to verify that they maintained a stable karyotype using the karyotyping technique. (A) Diagram of the procedure to obtain a pure culture of astrocytes-hNS1. (B) Representative micrographs of GFAP immunofluorescence in cultured astrocytes. Scale bar 50  $\mu\text{m}$ . (C) Reconstruction of the karyotype of three passages of astrocytes-hNS1.

**Fig 2. Astrocytes-hNS1 are permissible and susceptible to ZIKV infection.** (A) The astrocytes-hNS1 were seeded in 24-well plates and processed for immunofluorescence with antibodies against GFAP (green) and ZIKV envelope protein (red), and the nuclei were stained with Hoechst (blue). Scale bar 50  $\mu\text{m}$ . (B) The number of cells positive for ZIKV infection was quantified at three dpi with MOI of 1 (mean percentage and standard deviation,  $n=6$ ,  $p=0.031$ , t-test). (C) The Astrocytes were infected with ZIKV (MOI of 1), and supernatants were recovered for 5 dpi to determine viral genome production by qRT-PCR. An increase in the viral genome during the infection progress is shown (\* $p<0.05$ , \*\* $p<0.01$ , \*\*\* $p<0.001$ , ANOVA with Tukey's multiple comparisons). Each point represents the mean of 3 independent experiments with at least two duplicates, and the error bars correspond

to the standard deviation. (D) Brightfield microscopy of ZIKV infected (MOI of 1) or mock-infected astrocytes-hNS1 at 5 dpi. Scale bar 100  $\mu$ m. White arrows indicate cytopathic effect (E) Thin-section TEM of infected cells (MOI of 1) at 6 dpi shows the presence of viral particles inside vesicles (white arrows).

**Fig 3. ZIKV infection of astrocytes modifies the metabolic activity and the production of species reactive oxygen.** (A) Astrocytes-hNS1 were infected with ZIKV (MOI of 0.1 and 1), and at five dpi, viability was determined by indirectly measuring activity metabolism with resazurin. (B) The production of ROS was measured in mock-infected and ZIKV-infected cells at MOI of 0.1 and 1. In A and B, the data are median and interquartile range,  $n=3-4$ ,  $**p<0.01$ ,  $***p<0.001$ , Kruskal Wallis with Dunn's post hoc. For A and B,  $H_2O_2$  was used to induce cell death.

**Fig 4. Glial marker expression is altered by ZIKV infection.** The astrocytes-hNS1 culture was infected with ZIKV (MOI of 1) or mock-infected. At five dpi the cellular RNA was recovered and the expression of glial transcripts was analyzed by qRT-PCR. (A) Relative expression of GFAP in infected and uninfected cells,  $p=0.002$ ,  $n=6$ , t-test. (B) Relative expression of EAAT1,  $p=0.0006$ ,  $n=6$ , t-test. (C) Relative expression of GS,  $p=0.023$ ,  $n=6$ , t-test. (D) Relative expression of EAAT2,  $p=0.0006$ ,  $n=6$ , t-test. (E) Relative expression of CX43,  $p=0.10$ ,  $n=6$ , U Mann Whitney test. (F) Relative expression of  $NMDA_R$ ,  $p=0.0045$ ,  $n=6$ , t-test. The plotted data represent the mean and standard deviation.

**Fig 5. ZIKV infection can modify genes of the TAM family and genes involved in the lipidic metabolism.** The astrocytes-hNS1 culture was infected with either ZIKV (MOI of 1) or mock-infected. At five dpi, the cellular RNA was recovered and the relative expression of the mRNAs for the receptors of the TAM family (Tyro-3,

AXL, and Mertk), and APOE and PPAR $\gamma$  mRNAs associated with lipid metabolism were determined by qRT-PCR. (A) Tyro-3 relative expression,  $p=0.025$ ,  $n=6$ , t-test. (B) Relative expression of AXL,  $p=0.0022$ ,  $n=6$ , U Mann Whitney test. (C) Relative expression of Mertk,  $p=0.0006$ ,  $n=6$ , t-test. (D) Relative expression of PPAR- $\gamma$ ,  $p=0.24$ ,  $n=6$ , t-test. (E) APOE relative expression  $p=0.18$ ,  $n=6$ , t-test. The data correspond to the mean and standard deviation.

**Fig 6. Virions generated after ZIKV infection are concentrated in vesicles.** The astrocytes-hNS1 culture was infected with ZIKV (MOI of 1) or mock-infected. At 6 dpi, the monolayers were fixed and processed for observation by transmission electron microscopy. (A) Representative micrograph of an entire astrocyte-Hns1. Cells are characterized by large multilamellar bodies (see blue arrows). (B) ZIKV-infected cells at 6 dpi showed many vacuoles (see red arrows) and the multilamellar bodies were very rare in infected cells and were small (see blue arrows). (C) ZIKV-infected cells, where virions delimited in vesicles are observed (see green arrows). (D) ZIKV-infected cells show multiple Virions associated with vesicular bodies and close to the endoplasmic reticulum.

**Fig 7. ZIKV infection in astrocytes-hNS1 causes changes in the mitochondria.** The astrocyte-hNS1 culture was infected with ZIKV (MOI of 1) or mock-infected. The monolayers were fixed at 3 and 6 dpi and processed for observation by transmission electron microscopy. (A) Mock-infected cells at three dpi. (B) Mock-infected cells at six dpi. The mitochondria of the mock-infected cells show the homogeneous size and parallel cristae. (C) ZIKV-infected cells during 3 dpi showing mitochondria with concentric cristae and mitochondria with the sparse

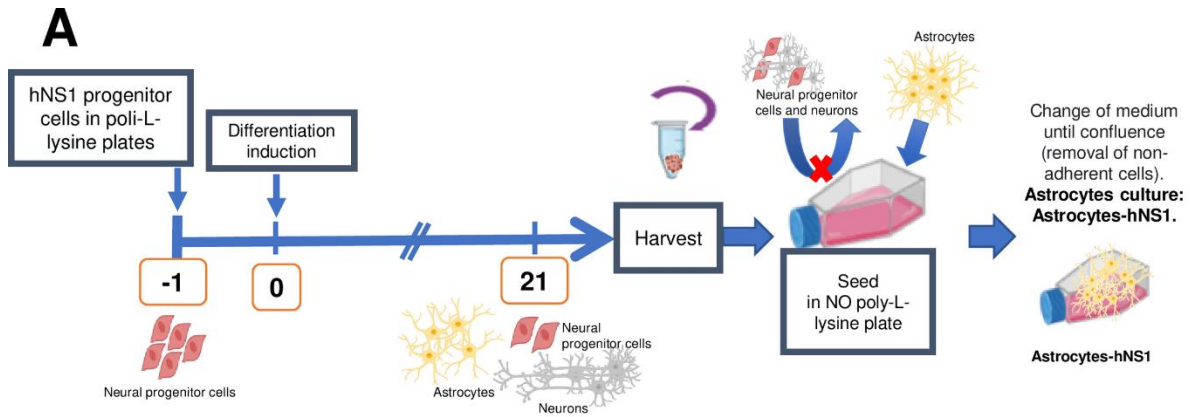


mitochondrial matrix. (D) ZIKV-infected cells 6 dpi showed decreased mitochondrial cristae and lighter electron density. (E) Quantitative analysis of the number of mitochondria per cell, the mean and standard deviation are presented,  $p=0.06$ , ANOVA. (F) Quantitative analysis of the size of the mitochondria expressed in the mitochondrial area ( $\mu\text{m}^2$ ), the median and range are presented,  $p<0.0001$ , Kruskal Wallis test with a post hoc Dunn's Multiple Comparison Test. In order to compare the area of the mitochondria we only analyzed organelles with the same orientation.

**Fig 8. ZIKV infection in astrocytes-hNS1 causes changes in lipid droplets (LDs).** The astrocyte-hNS1 culture was infected with ZIKV (MOI of 1) or mock-infected. At 3 and 6 dpi, the monolayers were fixed and processed for observation by transmission electron microscopy. (A) Mock-infected cells at three dpi. (B) Mock-infected cells at six dpi respectively, LDs can be observed in the cell's cytoplasm. (C) ZIKV-infected cells (MOI of 1) at three dpi showed many LDs throughout the cytoplasm. (D) Representative micrograph of a ZIKV-infected cell at six dpi showing abnormal mitochondria and a complete absence of LDs. (E) Quantitative analysis of the number of LDs /cells, median, and range are presented,  $**p<0.001$ ,  $***p<0.0001$ , U Mann Whitney test. (F) Quantitative analysis of LDs size (area,  $\mu\text{m}^2$ ), the mean and standard deviation are presented,  $p=0.10$ , Kruskal Wallis test, comparisons between the groups where measurements of LDs area could be determined.

# Figures

Fig 1. Astrocytes-hNS1 are a pure culture of human astrocytes.

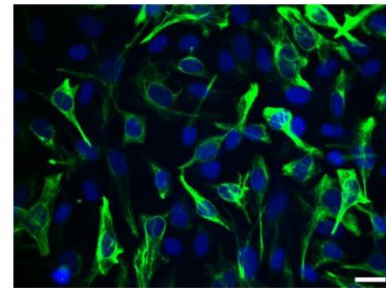
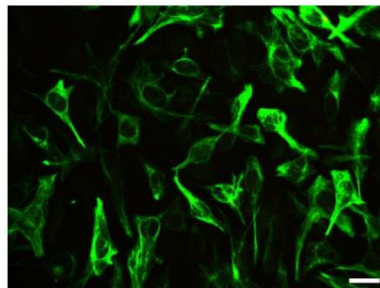
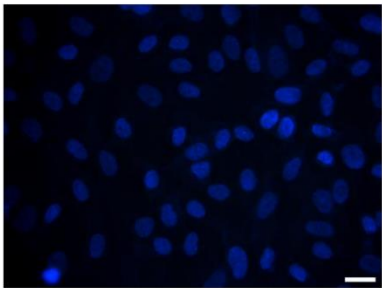


**B**

Nuclei

GFAP

Nuclei/GFAP



**C**

Astrocytes passage 10.

Astrocytes passage 15.

Astrocytes passage 22.

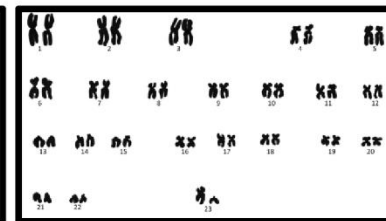
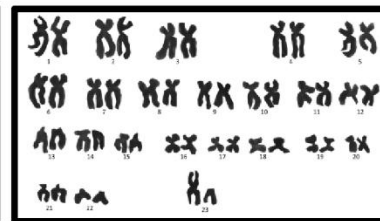


Fig 2. Astrocytes-hNS1 are permissible and susceptible to ZIKV infection.

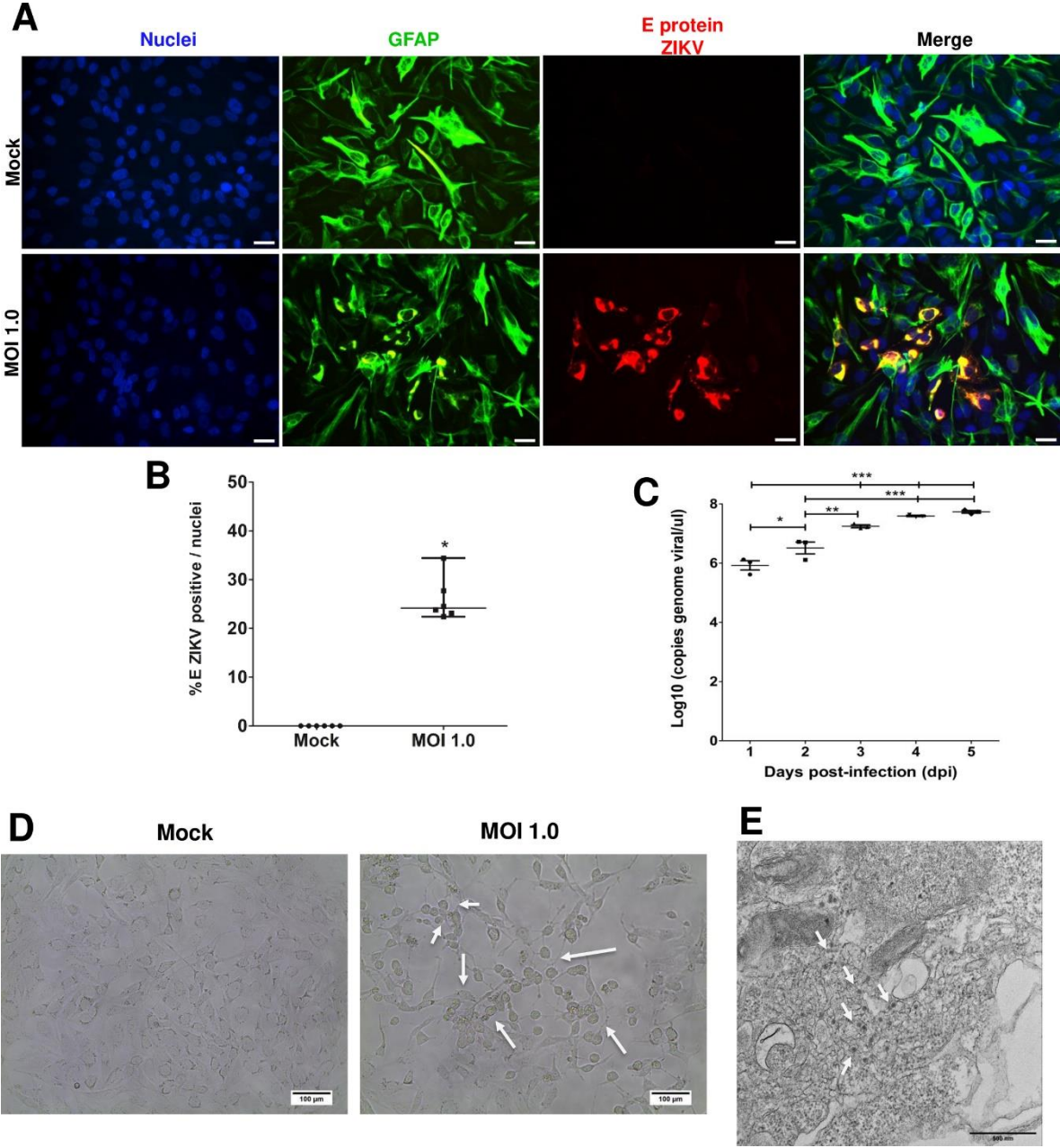
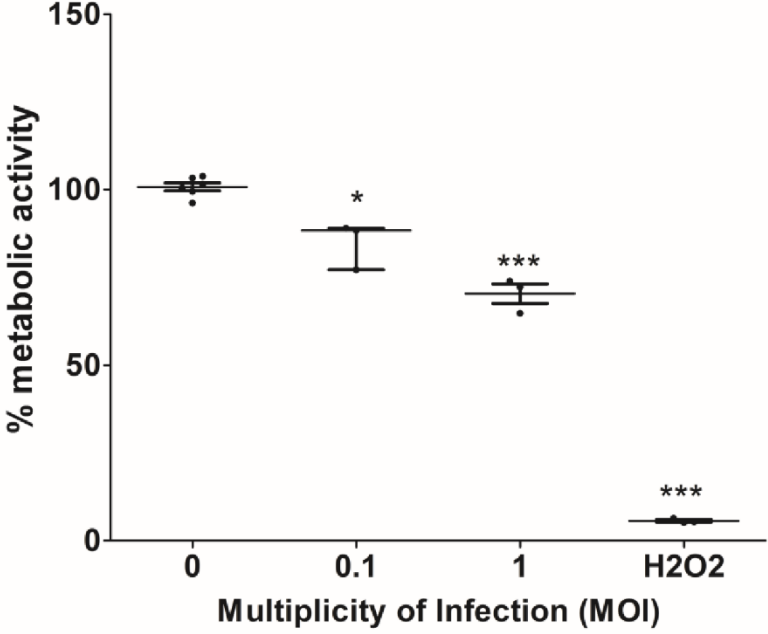


Fig 3. ZIKV infection of astrocytes modifies the metabolic activity and the production of species reactive oxygen.

**A**



**B**

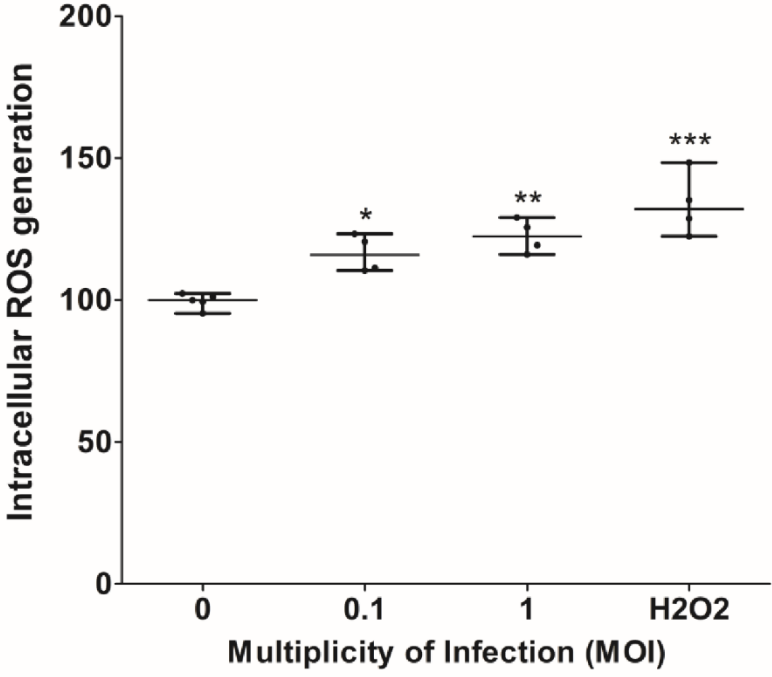


Fig 4. Glial marker expression is altered by ZIKV infection.

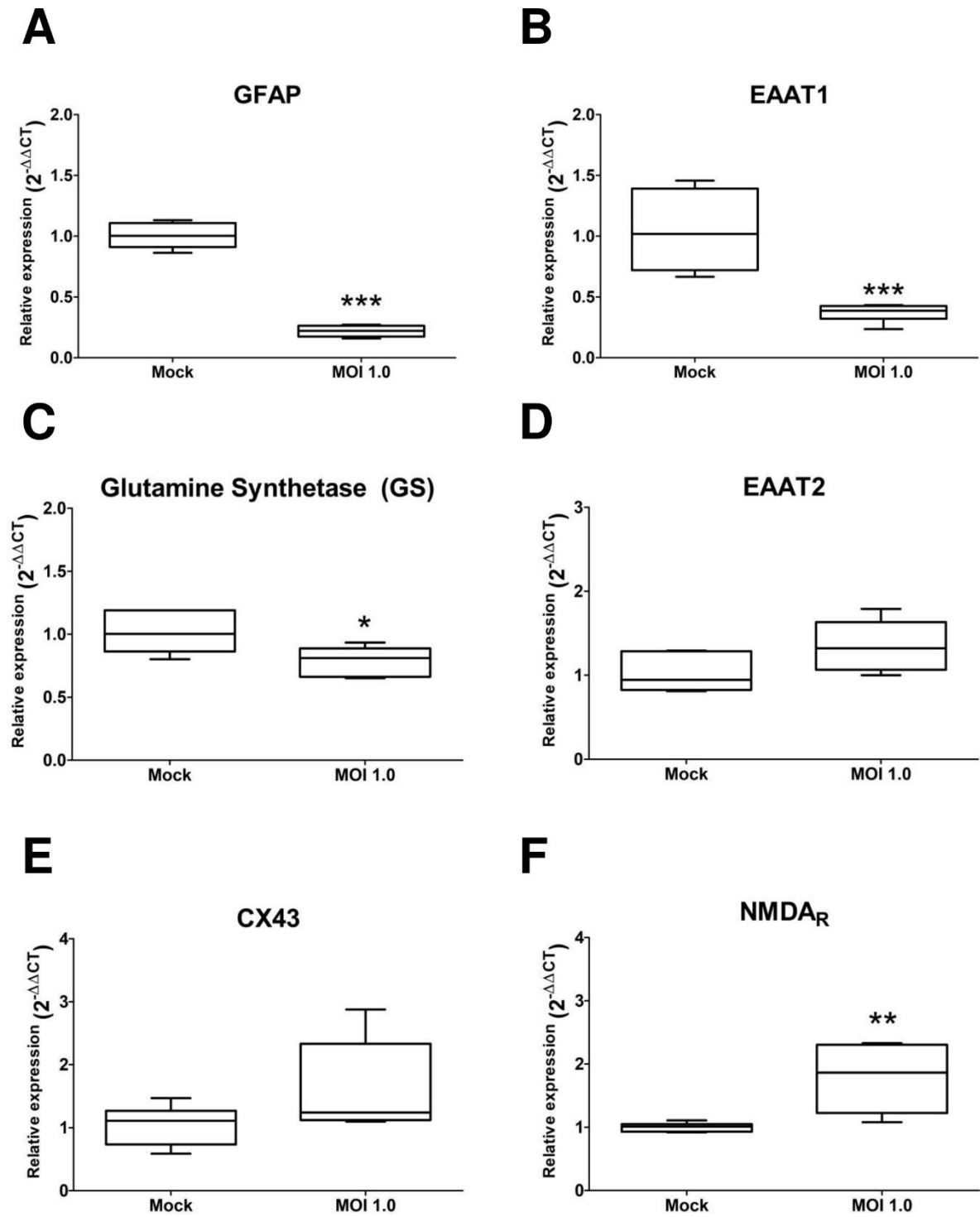


Fig 5. ZIKV infection can modify genes of the TAM family and genes involved in the lipidic metabolism.

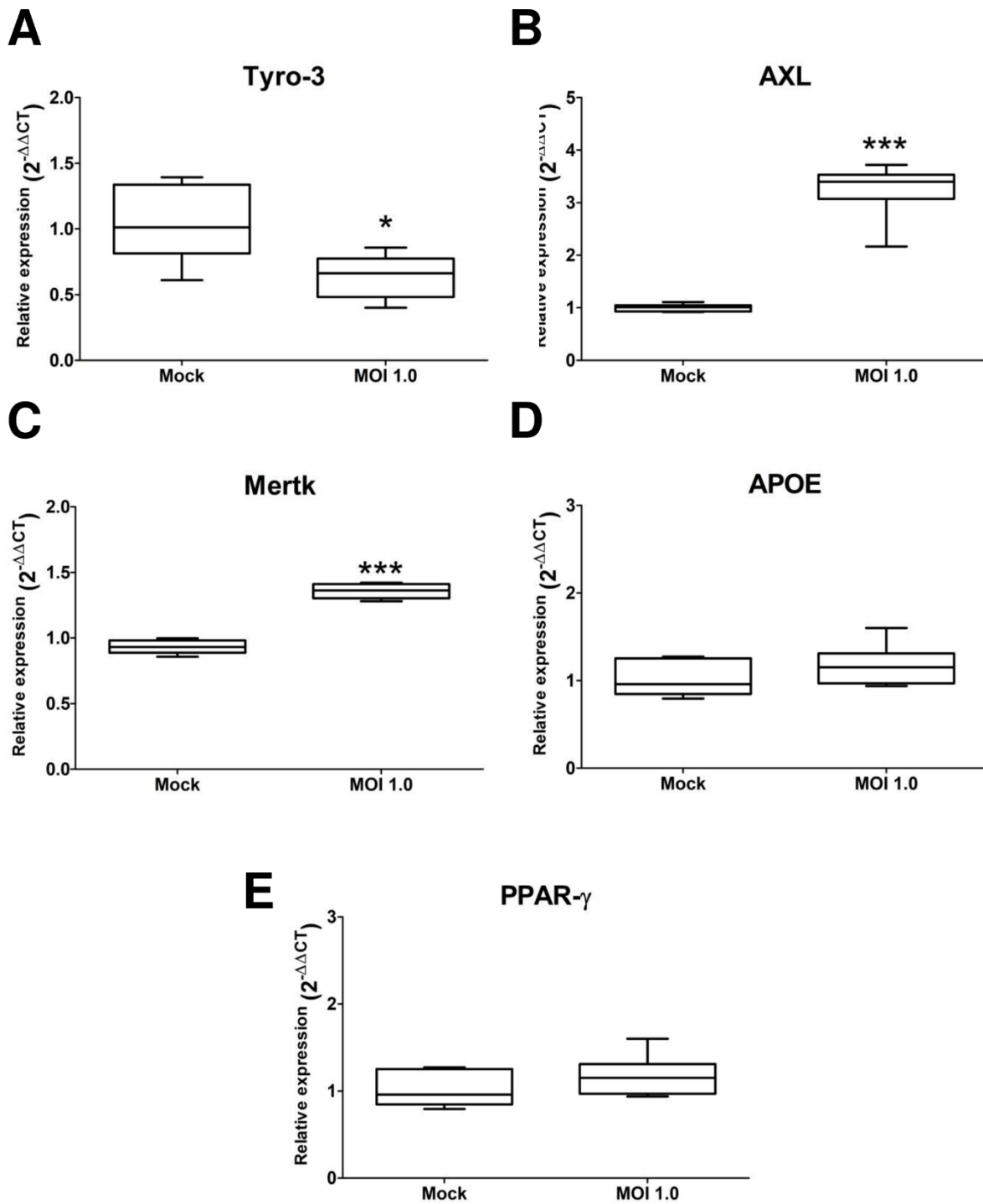




Fig 6. Virions generated after ZIKV infection are concentrated in vesicles.

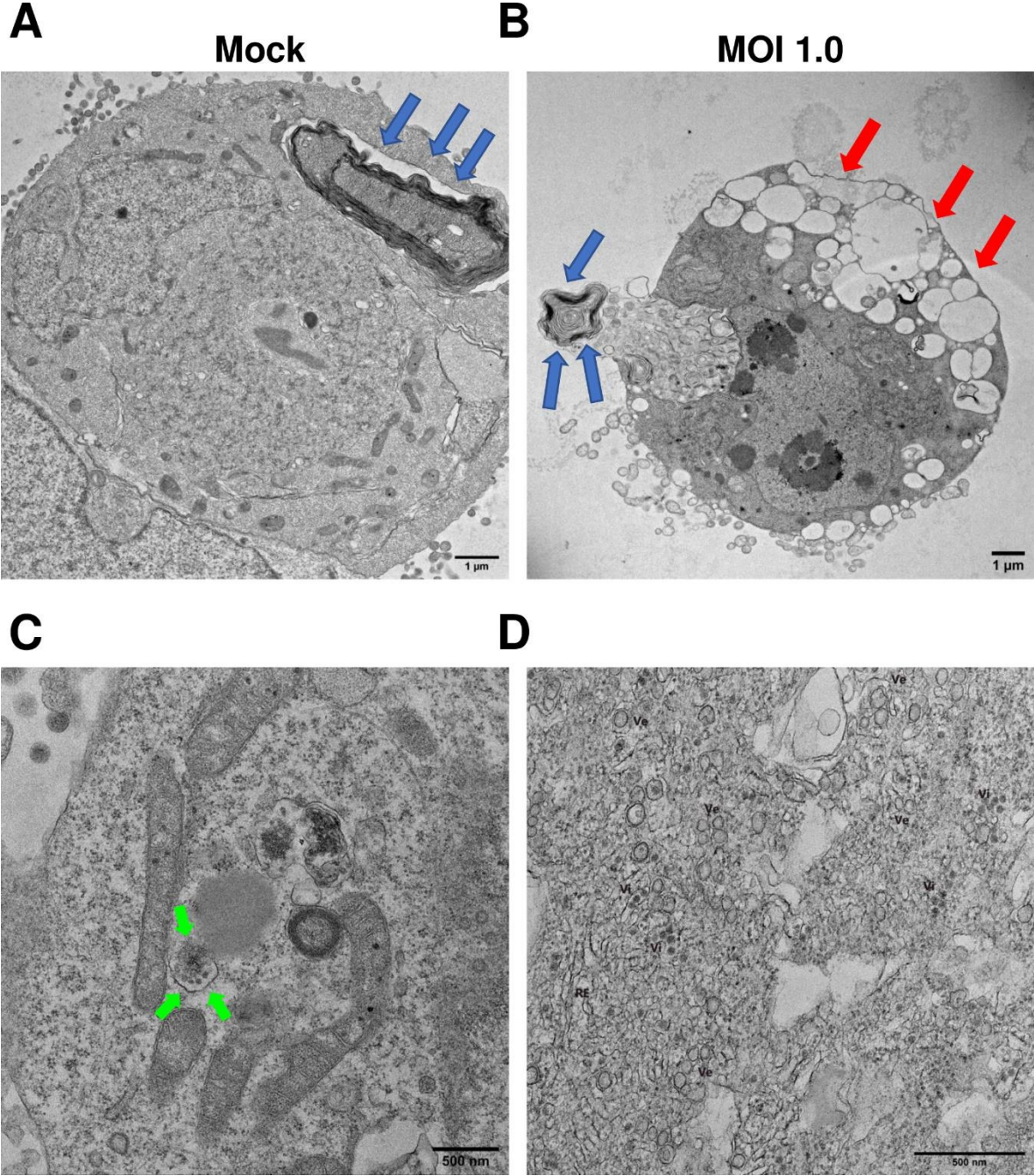


Fig 7. ZIKV infection in astrocytes-hNS1 causes changes in the mitochondria.

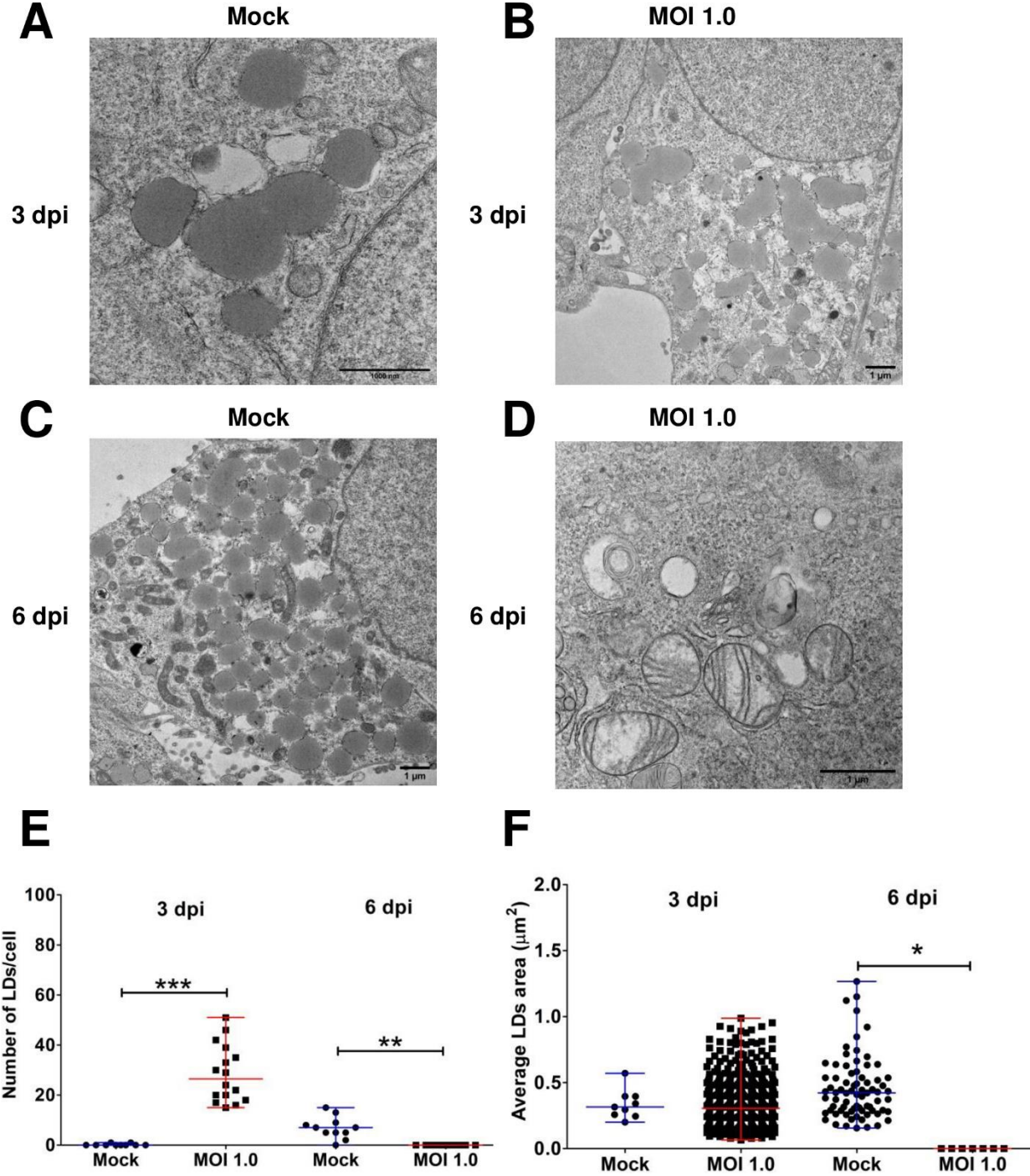
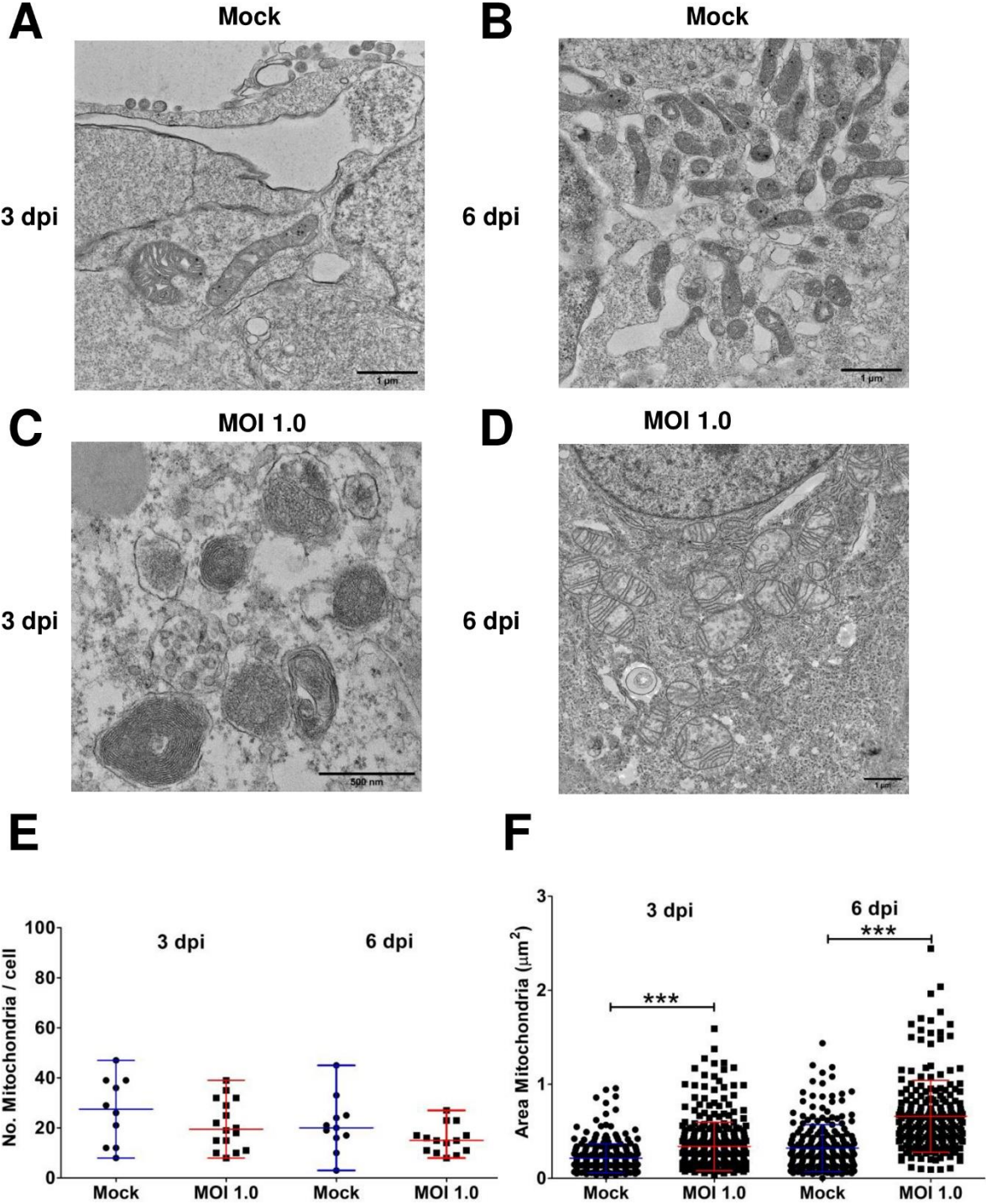
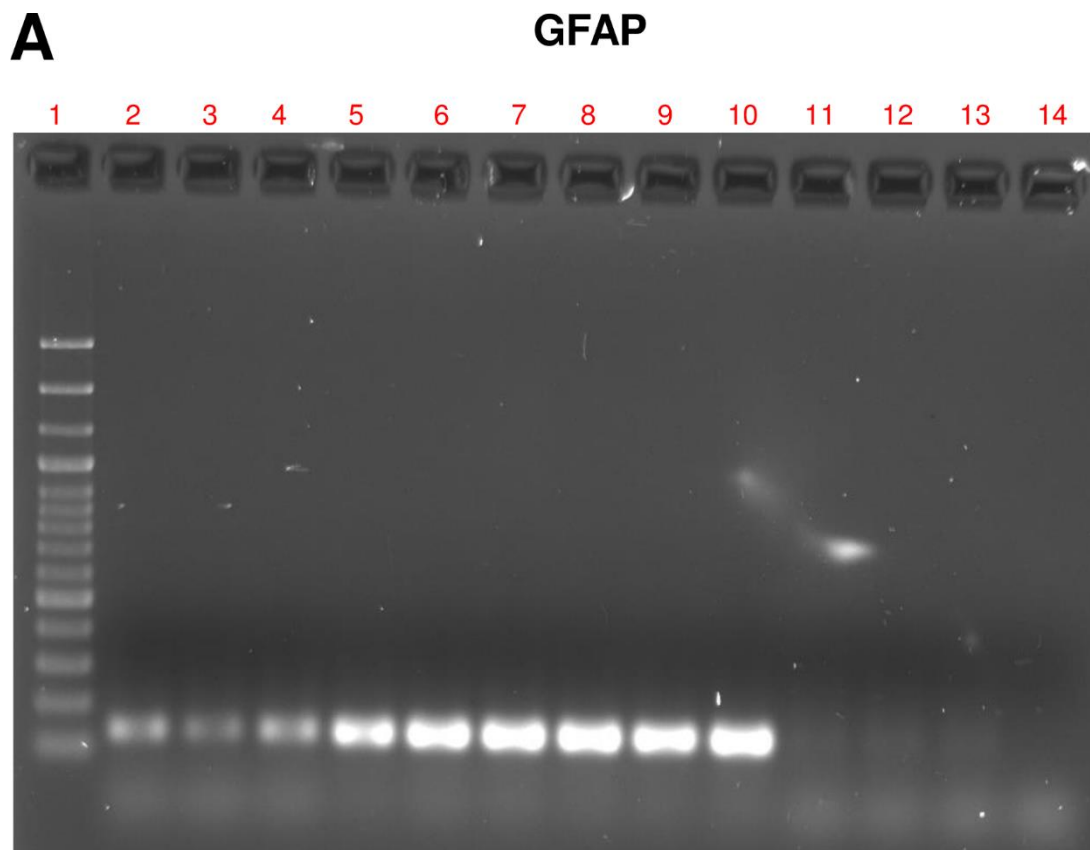




Fig 8. ZIKV infection in astrocytes-hNS1 causes changes in lipid droplets (LDs).



## Supporting information



1: Molecular weight Ladder

2-10: Different astrocyte cultures (celular pass 11,17 y 21)

11-13: Undifferentiated hNS1 cells (celular pass 27)

**S1 Fig Gene expression of glial cell marker GFAP in cultured astrocytes-hNS1 by One-step RT-PCR.** The astrocytes-hNS1 culture was seeded. At three days of proliferation, cellular RNA was recovered by analyzing the expression of gene markers of glial cells. Expression of GFAP in cells astrocytes-hNS1 and hNS1 cell line.

**S1 Table. The Primers used for PCR.** Primers used and their characteristics.

GENE	ENCODED	PRIMERS SEQUENCE (5'-3')		AMPLICON
<i>APOE</i>	APOE	FORWARD	GGAAGGCTAACCTGGGACTG	198
		REVERSE	ATCCCAAAGCGACCCAGTG	
<i>AXL</i>	AXL	FORWARD	GCTTCGGGATGGACAGATCC	216
		REVERSE	AAGTAAGGCAAGCCCTCCAG	
<i>GJA1</i>	CX43	FORWARD	CAAAATCGAATGGGGCAGGC	136
		REVERSE	GCTGGTCCACAATGGCTAGT	
<i>SLC1A3</i>	EAAT1	FORWARD	CGCCATCTTTATAGCCCAA	139
		REVERSE	CAGAATGAGGAGCATGGTGA	
<i>SLC1A2</i>	EAAT2	FORWARD	CATGCACAGAGAAGGCAAAA	210
		REVERSE	AGAGTCTCCATGGCCTCAGA	
<i>GAPDH</i>	GAPDH	FORWARD	CAAGGCTGAGAACGGGAAGC	194
		REVERSE	AGGGGGCAGAGATGATGACC	
<i>GFAP</i>	GFAP	FORWARD	ACATCGTGGTGAAGACCGTG	142
		REVERSE	CTATCCTGCTTCTGCTCGGG	
<i>GLUL</i>	GS	FORWARD	GCTGGTGTAGCCAATCGTAGC	123
		REVERSE	GGCTTCTGTCACCGAAAAGG	
<i>MERTK</i>	MERTK	FORWARD	AAATCCCCCTCCGTGCTAAC	129
		REVERSE	TGGGGAGGGAATTGCTTTGAT	
<i>GRIN1</i>	NMDAR	FORWARD	AGCTTCTACAACACCGAGGC	203
		REVERSE	GAGGCGTACACGATCTCCAG	
<i>PPAR-γ</i>	PPAR-γ	FORWARD	GCCTTAACCTCTGCTGGTGA	140
		REVERSE	TCGTAAAGGCTGACTCTCGTT	
<i>TYRO-3</i>	TYRO-3	FORWARD	GACTGGTCTGAGAGGGTGA	226
		REVERSE	CCCATGAGCTTCAGACCCTTT	
<i>ZIKV (non-structural protein 1, NS1)</i>	ZIKV (non-structural protein 1, NS1)	FORWARD	GAGTGTGATCCAGCCGTTATT	105
		REVERSE	CAGCCTCCATGTGTCATTCT	

# Other contributions

## Chapter 1

# Basic virological aspects of SARS-CoV-2

M. Comas-García<sup>1,2,3</sup>, E.I. Rubio-Hernández<sup>4</sup>, I. Lara-Hernández<sup>2</sup>, M. Colunga-Saucedo<sup>3</sup>, C.G. Castillo<sup>4</sup>, A. Comas-García<sup>3,5</sup>, A. Monsivais-Urenda<sup>6,7</sup> and R. Zandi<sup>8</sup>

<sup>1</sup>Department of Sciences, Autonomous University of San Luis Potosí, San Luis Potosí, Mexico, <sup>2</sup>High-Resolution Microscopy Section, Research Center for Health Sciences and Biomedicine, Autonomous University of San Luis Potosí, San Luis Potosí, Mexico, <sup>3</sup>Medical Genomics Section, CICSaB, UASLP, San Luis Potosí, Mexico, <sup>4</sup>Coordination for the Innovation and Application of Science and Technology (CIACYT)—Medical School, UASLP, San Luis Potosí, Mexico, <sup>5</sup>Department of Microbiology, Medical School, UASLP, San Luis Potosí, Mexico, <sup>6</sup>Translational Medicine Section, CICSaB, UASLP, San Luis Potosí, Mexico, <sup>7</sup>Department of Immunology, Medical School UASLP, San Luis Potosí, Mexico, <sup>8</sup>Department of Physics and Astronomy, University of California, Riverside, CA, United States

## 1.1 Introduction

Coronaviruses (CoVs) belong to a group of positive-sense single-stranded RNA viruses that have the largest genome known for a virus and use RNA as its genetic material. These viruses can infect a wide variety of animals, causing very different diseases that include common cold (humans), peritonitis (cats), hepatitis (mouse), and life-threatening pneumonia (humans). In fact, before the year 2002, most of CoV literature focused on viruses of veterinarian interest. This changed in 2002 and 2012 with the appearance of two novel human CoVs that cause Severe Acute Respiratory Syndromes, SARS-CoV and MERS-CoV, respectively. The localized epidemics caused by these two viruses served as warning events on how zoonotic transmission of CoVs between bats (or camels) and humans could result in the formation of new viruses. Unfortunately, the research on these viruses mostly caught only the attention of the groups that either previously worked with CoVs of veterinarian interest or lived in the regions affected by SARS-CoV and MERS-CoV.




The emergence of a novel human CoV (SARS-CoV-2) in Wuhan, China at the end of 2019 changed the world. By the first trimester of 2020, this virus was almost in every continent, causing an unprecedented halt of social, academic, economic, cultural, sports, and even political activities. This pandemic not only changed the way we behave but also the way science is done. Since the release of the first full-length SARS-CoV-2 genome, in February of 2020 by the group of Prof. Zhang (Wu et al., 2020), research groups from all around the world decided to learn about CoVs and develop new research interests. Most importantly, in order to fight this pandemic, we need to develop new biomedical and biotechnological tools to understand, at least at a basic level, how CoVs (especially SARS-CoV-2) function.

The goal of this chapter is to establish the minimal virological basis required to understand the viral infectious cycle. It is not our intention to provide a detailed review of every single aspect of the viral infectious cycle but to highlight key parts of it. In fact, we apologize to everyone whose work has not been highlighted. This chapter is intended to help the reader navigate through the rest of the book and to appreciate the novel biotechnological approaches that have been developed to fight the COVID-19 pandemic. This chapter presents the different steps of the viral infectious cycle as it occurs in the cell. First, we introduce the virus by giving a description of the genome organization and the function of some of its genes; afterward, we address virion entry, replication, assembly, and egress. Finally, we added a section regarding the immune response to a viral infection. The goal of this section is to provide the readers with the minimal knowledge required to understand and appreciate the rest of the chapters.



## Article

# Construction of a Chikungunya Virus, Replicon, and Helper Plasmids for Transfection of Mammalian Cells

Mayra Colunga-Saucedo <sup>1</sup>, Edson I. Rubio-Hernandez <sup>2</sup>, Miguel A. Coronado-Ipiña <sup>3</sup>,  
Sergio Rosales-Mendoza <sup>4,5</sup>, Claudia G. Castillo <sup>2</sup> and Mauricio Comas-García <sup>1,3,6,\*</sup>

- <sup>1</sup> Sección de Genómica Médica, Centro de Investigación en Ciencias de la Salud y Biomedicina, Universidad Autónoma de San Luis Potosí, San Luis Potosí 78210, Mexico
  - <sup>2</sup> Laboratorio de Células Troncales Humanas, Coordinación para la Innovación y Aplicación de la Ciencia y la Tecnología, Facultad de Medicina, Universidad Autónoma de San Luis Potosí, San Luis Potosí 78210, Mexico
  - <sup>3</sup> Sección de Microscopía de Alta Resolución, Centro de Investigación en Ciencias de la Salud y Biomedicina, Universidad Autónoma de San Luis Potosí, San Luis Potosí 78210, Mexico
  - <sup>4</sup> Sección de Biotecnología, Centro de Investigación en Ciencias de la Salud y Biomedicina, Universidad Autónoma de San Luis Potosí, San Luis Potosí 78210, Mexico
  - <sup>5</sup> Facultad de Ciencias Químicas, Universidad Autónoma de San Luis Potosí, San Luis Potosí 78210, Mexico
  - <sup>6</sup> Facultad de Ciencias, Universidad Autónoma de San Luis Potosí, San Luis Potosí 78295, Mexico
- \* Correspondence: mauricio.comas@uaslp.mx

**Abstract:** The genome of Alphaviruses can be modified to produce self-replicating RNAs and virus-like particles, which are useful virological tools. In this work, we generated three plasmids for the transfection of mammalian cells: an infectious clone of Chikungunya virus (CHIKV), one that codes for the structural proteins (helper plasmid), and another one that codes nonstructural proteins (replicon plasmid). All of these plasmids contain a reporter gene (mKate2). The reporter gene in the replicon RNA and the infectious clone are synthesized from subgenomic RNA. Co-transfection with the helper and replicon plasmids has biotechnological/biomedical applications because they allow for the delivery of self-replicating RNA for the transient expression of one or more genes to the target cells.

**Keywords:** Chikungunya virus; alphavirus DNA vectors; replicon plasmid; helper plasmid



**Citation:** Colunga-Saucedo, M.; Rubio-Hernandez, E.I.; Coronado-Ipiña, M.A.; Rosales-Mendoza, S.; Castillo, C.G.; Comas-García, M. Construction of a Chikungunya Virus, Replicon, and Helper Plasmids for Transfection of Mammalian Cells. *Viruses* **2023**, *15*, 132. <https://doi.org/10.3390/v15010132>

**Academic Editors:** Roya Zandi, Michael F. Hagan, Charlotte Uetrecht and Eric O. Freed

Received: 10 November 2022  
Revised: 9 December 2022  
Accepted: 28 December 2022  
Published: 31 December 2022



**Copyright:** © 2022 by the authors. Licensee MDPI, Basel, Switzerland.

## 1. Introduction

Chikungunya virus (CHIKV) belongs to the *Togaviridae* family and genus *Alphavirus*, and it is also known as an Arbovirus (Arthropod-borne virus) because it is transmitted by mosquitos from the genus *Aedes*. According to the European Centre for Disease Prevention and Control, in 2022, there were 338,592 confirmed cases and 70 deaths associated with CHIKV. The majority of cases were reported in Brazil (240,344), India (93,113), Guatemala (1435), Thailand (775), and Malaysia (662). A meta-analysis of 44 studies worldwide that included 51,599 people from 29 countries revealed that up to 25% of the population could be seropositive to CHIKV. The region with the highest prevalence was Southeast Asia, with 42%, and the lowest was the Eastern Mediterranean, with 2% [1]. CHIKV has a positive-sense, single-stranded RNA genome (gRNA) that is encapsulated in an T = 4 icosahedral virion. The virion is composed of a nucleocapsid containing 240 monomers of capsid protein, one copy of the gRNA, a lipid bilayer, and eighty trimers of a heterodimer of the glycoproteins E2/E1. The capsid proteins and glycoproteins interact with each other and

## Popular science publications



REVISTA  
Avance y Perspectiva



### ¿PODEMOS ERRADICAR ENFERMEDADES CON FÁBRICAS DE MOSQUITOS?

*Autor: EDSON IVÁN RUBIO HERNÁNDEZ*

*Enviado: 20 de Enero 2023. Publicado: 28 de Febrero 2023.*

**Categories:** [Ciencias Naturales y de la Salud](#), [Zona Abierta](#)

**Tag:** [Volumen 8 - Número 4](#)

Todos hemos notado lo desagradables que son los mosquitos: el zumbido cerca de nuestros oídos, y las picaduras y consecuentes ronchas o pequeñas ampollas que aparecen; lo más preocupante es que los mosquitos pueden estar infectados de bacterias o virus y transmitirlos al hombre a través de su picadura, ocasionando enfermedades mortales, por ejemplo, el Dengue hemorrágico.

Los mosquitos se han considerado como los animales más peligrosos del planeta debido a que pueden transmitir enfermedades graves y mortales, y son un desafío para la salud pública en el ámbito mundial.

En América Latina, tan solo en el año 2022, se notificaron 3,126,089 casos de enfermedades ocasionadas por arbovirus. Los arbovirus son un tipo de virus que se transmiten a los humanos y otros animales a través de las picaduras de mosquitos, garrapatas u otros artrópodos infectados. En lo que concierne a los 3 millones de casos asociados a arbovirosis, 90% fueron de Dengue, el 8.8% de Chikungunya y un 1.3% de Zika (Datos ingresados en la Plataforma de Información de Salud para las Américas -PLISA, PAHO / WHO-, 2023).

El caso más reciente que impactó al sistema de salud fue el del virus del Zika, que se descubrió en 1947, en el bosque de Zika en Uganda. Durante 60 años, sus infecciones en humanos fueron aisladas y poco documentadas. Sin embargo, en 2007 surgió una epidemia en la isla Yap, de la Micronesia; en 2013 brotó en la Polinesia Francesa; en 2014 el virus del Zika llegó a América Latina.

**Link de consulta:** <https://avanceyperspectiva.cinvestav.mx/podemos-erradicar-enfermedades-con-fabricas-de-mosquitos/>

# Slide presentation

UNIVERSIDAD AUTÓNOMA DE SAN LUIS POTOSÍ  
FACULTAD DE MEDICINA  
Centro de Investigación en Ciencias de la Salud y Biomedicina (CICSaB)

EFFECTO DE LA INFECCIÓN DEL VIRUS DE ZIKA EN LA DIFERENCIACIÓN NEURAL DE UNA LÍNEA CELULAR TRONCAL HUMANA

TESIS QUE PRESENTA  
M. C. EDSON IVÁN RUBIO HERNÁNDEZ  
PARA OBTENER EL GRADO DE DOCTOR EN CIENCIAS BIOMÉDICAS BÁSICAS

COMITÉ TUTORIAL: JURADO:

CODIRECTORES: DRA. CLAUDIA CASTILLO MARTÍN DEL CAMPO, DR. MAURICIO COMAS GARCÍA  
ASESORES INTERNOS: DRA. ADRIANA MONSIVAI URENDA, DR. CHRISTIAN GARCÍA SEPULVEDA  
ASESOR EXTERNO: DR. JOSÉ FERNANDO PEÑA ORTEGA

PRESIDENTE SINODAL: DR. DANIEL NOYOLA CHERPITEL  
SECRETARÍA DE SINODALES: DRA. ADRIANA MONSIVAI URENDA  
SINODALES: DRA. CATALINA PATRICIA PORTALES PÉREZ, DR. JOSÉ FERNANDO PEÑA ORTEGA  
SINODAL SUPLENTE: DRA. SARAY ARANDA ROMO

30 de Marzo 2023



## Introducción

### Virus Zika (ZIKV):

ZIKV es un arbovirus perteneciente a la familia *Flaviviridae*, del género *Flavivirus*.

ZIKV se aisló por primera vez del suero de un mono Rhesus en 1947.

Nombre del virus: Bosque de Zika en Uganda.

Proteína de envoltura (E)  
Proteína de membrana (M)  
Proteína de Cápside (C)  
ARN genómico

Sitios de corte de proteínas virales

(Barouch, et al. 2017; Ávila-Pérez et al. 2018)

## Introducción

### Manifestaciones clínicas de la infección por ZIKV:

Infección por ZIKV → Período de incubación (3-12 días) → Presentación de síntomas (18-20%, 2-7 días)

Transmisión vector *Aedes*  
Transmisión por contacto con fluidos corporales  
Transmisión sexual

Sintomatología

Brotos del 2015-2017:

- Asociado a enfermedad grave: Insuficiencia multigénica y trombocitopenia
- Síndrome de Guillain-Barré.
- Lesiones asociadas a infección congénita: lesiones en neurodesarrollo (microcefalia), malformaciones congénitas y muerte fetal.

Sigue siendo un problema de carácter mundial: Casos de ZIKV durante el 2022: 40,639 casos.

## Introducción

### Casos de ZIKV en mujeres embarazadas y microcefalia congénita:

Reportes en países latinoamericanos (Colombia)

Año	2015	2016
Nacidos	516,264	489,235
Casos de microcefalia	110	479
Prevalencia	2.1	9.8

Colombia (2015-2016): 8,165 casos de malformaciones relacionadas al SNC en recién nacidos. 1,638 casos vinculados a infección por ZIKV (20%).

Brasil (2015-2016): 10,867 casos de malformaciones relacionadas al SNC en recién nacidos. 2,366 casos vinculados a infección por ZIKV (21.8%).

Brasil: Ministerio de Saúde do Brasil (2016). Colombia: Instituto Nacional de Salud (2016).

## Introducción

### Panorama epidemiológico de la infección de ZIKV en México:

En México desde 2015 hasta 2023 hay 13,003 casos confirmados.

55% de los casos corresponden a mujeres embarazadas (7152 casos).

Desde 2015 hasta 2023: 54 casos de microcefalia y síndrome congénito asociados a ZIKV.

2021: 1574 casos de DTNDCF

15 diagnósticos con Arbovirosis (enfermedad causada por arbovirus, ZIKV, DENV y CHIKV).

Sistema de Vigilancia Epidemiológica de Defectos del Tubo Neural y Craneofaciales SINAVE/DGE/SaHd., 2020, 2021.

Sigue siendo un problema de carácter mundial: Casos de ZIKV en 2022: 40,639 casos.

Poco conocimiento sobre la neuropatogénesis tras la infección en el SNC en desarrollo.

Usos de sistemas *in-vivo* e *in-vitro* para estudio de ZIKV.

## Introducción

### Modelos animales para el estudio de la infección congénita por ZIKV:

Ratones C57BL/6 en gestación al día 13.5 → Se exponen los cuernos uterinos → Se inoculan 500 virus en ventriculos laterales de cada embrión.

Modelo de ratones deficientes de NFIR.

Inóculo de 10,000 virus por vía subcutánea.

Uso de ratonas hembras con 6, 9 y 12 días de gestación.

Fetus

FTU equivalent per g

Cuando hay menor tiempo de gestación, la susceptibilidad a ZIKV es mayor.

(Zhang et al., 2019; Jagger et al., 2017)



## Introducción

### Estudios *in-vitro* utilizando cultivo de células neurales

**Infección por ZIKV (Linaje asiático y linaje africano).**

Alta permisividad.				Baja permisividad.		
Células progenitoras neurales.	Células progenitoras neurales.	Neuronas inmaduras y maduras.	Células gliales maduras.	Células gliales maduras.	Neuronas inmaduras.	Neuronas maduras.
Tang et al. 2016. Nguyen et al. 2016. Li et al. 2016.	Hughes et al. 2016. Russo et al. 2017. Li et al. 2016.	Qian et al. 2016. Fernandes et al. 2016. Fernandes et al. 2016.	Tang et al. 2016. Rostlack, 2016. Fernandes et al. 2016.	Nguyen et al. 2016. Eugenin et al. 2022.	Tang et al. 2016. Nguyen et al. 2016.	Hughes et al. 2016. Rostlack, 2016.

**Diferencias en los resultados:**

- Uso de la cepa de linaje Africano de ZIKV
- Diferentes grados de desarrollo neural en los sistemas de cultivo celular (poco caracterizados)
- Cultivos celulares desarrollados a partir de tumores

**Problemas experimentales trabajando con células progenitoras neurales:**

La diferenciación se restringe a la generación de neuronas o glia.

**Línea celular hNS-1. Células progenitoras neurales humanas**

[7]

## Introducción

### Células progenitoras neurales humanas Línea celular hNS-1

Células obtenidas de tejido fetal humano (10.5 semanas). Región: Diencefalo y Telencefalo.

Immortalización con el oncogén *v-myc*. Expresión condicionada a EGF y FGF.

**Células en proliferación.**  
Células cultivadas en medio con EGF y FGF: expresan Vimentina y Nestina.

**Células en diferenciación.**  
Células cultivadas en medio sin EGF y FGF: Comienzan a presentarse Neuronas y astrocitos en el cultivo.

ICQ Vimentina  
RT-PCR Nestina MPM

EGF FGF  
Proliferación  
Diferenciación

V-myc

(Villa, et al. 2004)

[8]

## Introducción

### Caracterización de línea celular hNS-1 en distintos estadios de diferenciación:

**Neuronas.**

MAP-2/Hoechst Day 1, Day 3, Day 5, Day 7, Day 11, Day 21

**Astrocytes.**

GFAP/Hoechst Day 1, Day 3, Day 5, Day 7, Day 11, Day 21

**Modelo idóneo de estudio de la neuroinfección de ZIKV en distintas etapas de la diferenciación.**

MAP-2  
% Células MAP-2+  
Días de diferenciación

GFAP  
% Células GFAP+  
Días de diferenciación

Progenitor neural  
Neuronas  
Oligodendrocytes  
Astrocytes

Progenitor glial  
Astrocytes

González-Sánchez et al. 2023, en preparación.

[9]

## Justificación:

- Los casos de microcefalia y malformaciones del Sistema Nervioso Central (SNC) asociados a la infección por ZIKV en mujeres embarazadas son un problema de salud mundial urgente.
- En México siguen existiendo un mayor número casos de defectos en el neurodesarrollo a los presentados antes del 2016 (Introducción de ZIKV en América Latina).
- Son necesarios estudios que aporten conocimientos básicos que nos ayuden a entender los efectos sobre las células del SNC producidos por la infección de ZIKV.
- En un futuro sea posible generar tratamientos, establecer un mecanismo claro de la pérdida neuronal y saber si es posible realizar algunas intervenciones durante el embarazo que puedan prevenir el daño cerebral.

[10]

## Pregunta de investigación:

¿Las células hNS-1 infectadas con ZIKV en distintos estadios de diferenciación (sin diferenciar, diferenciadas y una población aislada del cultivo diferenciado) presentarán distinta actividad metabólica, estrés oxidativo y carga viral?

## Hipótesis:

Los efectos provocados (actividad metabólica, estrés oxidativo y la carga viral) tras la infección del ZIKV en las células hNS-1 dependerá del grado de diferenciación del cultivo (sin diferenciar, diferenciadas y una población aislada de cultivo diferenciado)

[11]

## Objetivo General:

- Analizar en que grado de diferenciación los cultivos de la línea celular hNS-1 (sin diferenciar, diferenciados, una población una población aislada del cultivo diferenciado) son más susceptibles a la infección de ZIKV de linaje asiático.

## Objetivos específicos:

- Obtener stocks virales de ZIKV a partir de un plásmido de expresión de células de mamífero
  - Transfección de plásmido ICD en células HEK-293T.
  - Producción de stock de ZIKV en células Vero-E6
  - Conteo en placa.
- Determinar si el tropismo de ZIKV está influenciado por el estado de diferenciación neural.
  - Actividad metabólica.
  - Producción de ROS.
  - Cinéticas de producción viral.
  - Cinéticas de producción viral.
- Determinar cambios en la diferenciación de las células hNS-1 cuando se infectan con ZIKV.
  - PCR tiempo real de marcador glial (GFAP).
  - PCR tiempo real de marcador neuronal ( $\beta$ -tubulina III)
- Analizar la infección de ZIKV en células maduras (astrocytes) derivadas de la línea celular hNS-1.
  - Viabilidad celular.
  - Producción de ROS.
  - Cinéticas de producción viral.
  - PCR tiempo real.

[12]



**Materiales y Métodos** Objetivo 1: Obtener stocks virales de ZIKV.

## Plásmido ZIKV-ICD para la obtención de Stocks virales:

Amplificación de plásmido en bacterias → Purificación de plásmidos con columnas → Transfección de plásmidos en células de mamífero → Generación de partículas virales de ZIKV por células de mamífero

Plásmido ICD evita trabajar con muestras clínicas, y la partículas virales infecciosas son idénticas al aislado clínico de Paraíba, Brasil, 2015.

(Tsatsarkin, et al. 2016)

**Materiales y Métodos** Objetivo 1: Obtener stocks virales de ZIKV.

## Plásmido ZIKV-ICD para la obtención de Stocks virales:

**Transfección con el método de fosfato de Calcio:**

Siembra de células HEK-293T → Preparación de partículas de Calcio con plásmido ICD → Se quitan las partículas ADN-Calcio y se agrega medio → Incubación durante 16 hrs → Se cambia el medio durante 4 días, y el medio es recuperado y filtrado Para infectar células VERO-E6

**Infección de células Vero-E6 con sobrenadantes de HEK-293T transfectadas:**

Siembra de células Vero-E6 → Dilución de sobrenadantes de HEK-293T transfectadas con ZIKV-ICD → Se agrega medio fresco → Incubación durante 2 hrs → El medio de cultivo es recuperado y filtrado Stock de ZIKV producido en células VERO-E6

**Materiales y Métodos** Objetivo 1: Obtener stocks virales de ZIKV.

## Plásmido ZIKV-ICD para la obtención de Stocks virales:

**Ensayo en placa para la cuantificación del Stock viral:**

Stock viral → 1000 µl, 500 µl, 250 µl, 125 µl, 62.5 µl, 31.25 µl, 15.6 µl, 7.8 µl → 900 µl de solución buffer → Se infectan monocapas de células Vero-E6 → Incubación por 2 horas → Se retira inóculo → Se agrega medio con carboxi-metil celulosa 1.6% (virus no difunden a otros sitios, solo a células contiguas) → Incubación durante 4 días → Fijación de células con formaldehído Tinción con cristal violeta → Conteo de placas en dilución que lo permita. → Cálculo de partículas virales/ml: Teniendo en cuenta que una partícula viral al infectar generó una placa.

**Resultados** Objetivo 1: Obtener stocks virales de ZIKV.

## Producción de stock de ZIKV con altos títulos virales

Transfección de células HEK-293T con el plásmido ZIKV-ICD. → Infección de células Vero-E6 con sobrenadantes de células HEK-293T transfectadas con ZIKV-ICD. → Cuantificación de stock de ZIKV con ensayo en placa.

Células HEK-293T. 3 días post-transfección ZIKV-ICD. (Control vs Plásmido ZIKV-ICD)

Células Vero-E6 infectadas con ZIKV ICD. (Mock vs 4 días post-infección (dpi))

Cuantificación de Stock viral por ensayo en placa

Stock viral de ZIKV generado en células Vero-E6:  $1.34 \times 10^7 \frac{UFP}{mL}$

UFP: Unidades formadoras de placa

**Materiales y Métodos** Objetivo 2: Tropismo de ZIKV es influenciado por el estado de diferenciación

## Infección de ZIKV en células hNS-1 en un estado inmaduro:

Progenitor neuronal → Proliferación → Progenitor neuronal → Progenitor glial → Neuronas, Oligodendrocitos, Astrocitos

**A** Infección de ZIKV con distintas MOI (0.01, 0.1 y 1) → Células inmaduras → Medio proliferación → Células inmaduras

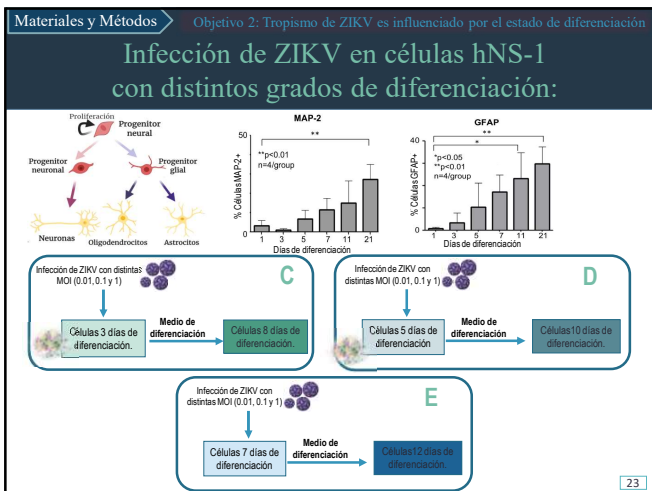
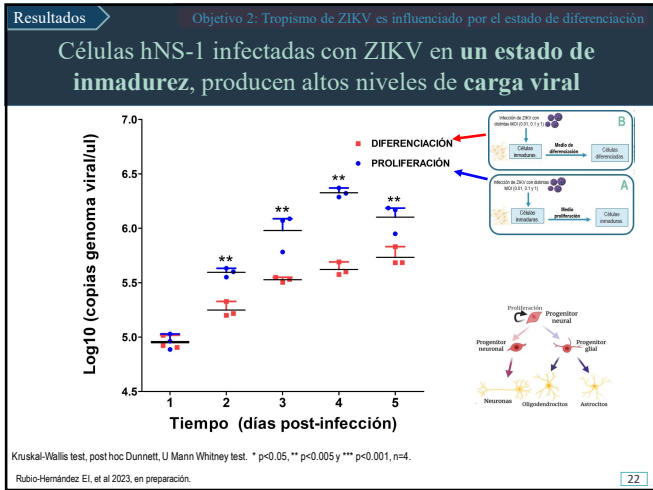
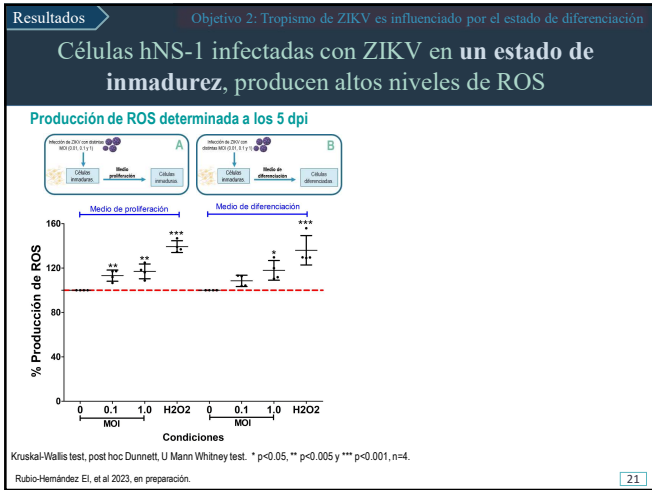
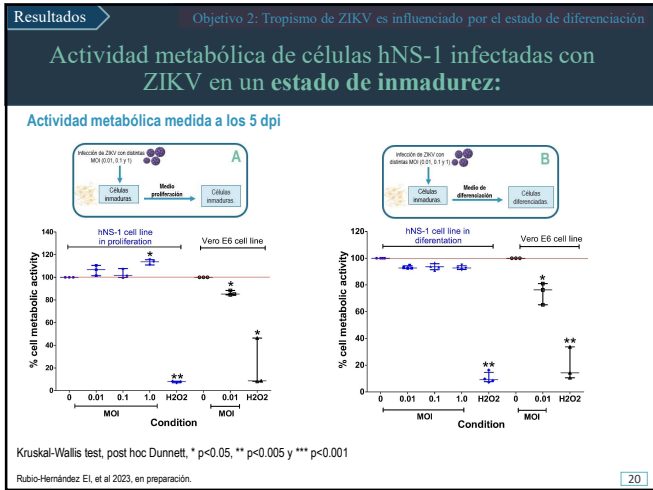
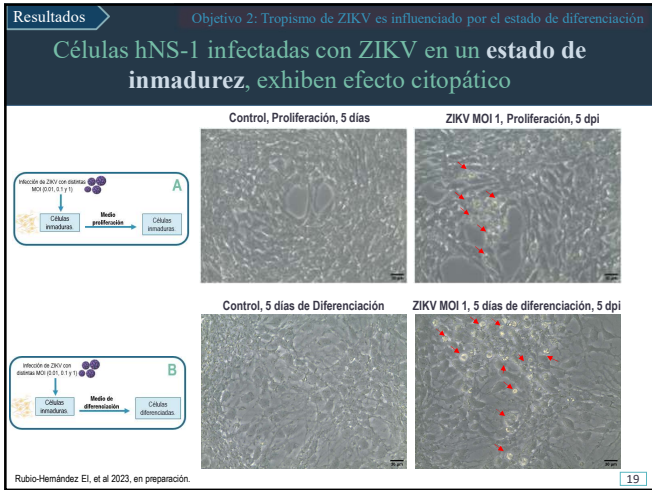
**B** Infección de ZIKV con distintas MOI (0.01, 0.1 y 1) → Células inmaduras → Medio de diferenciación → Células diferenciadas

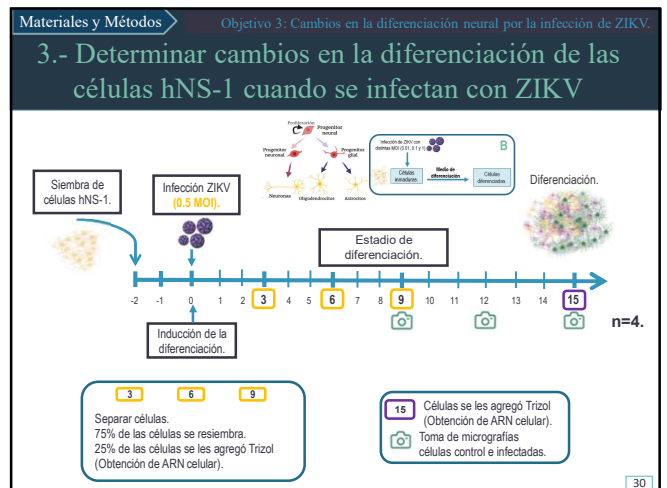
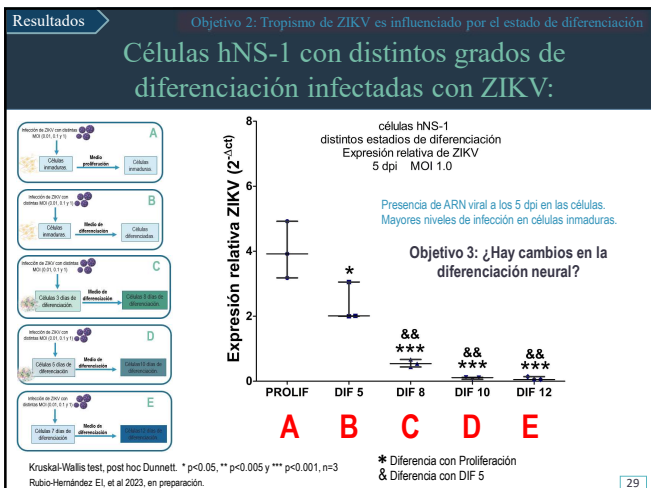
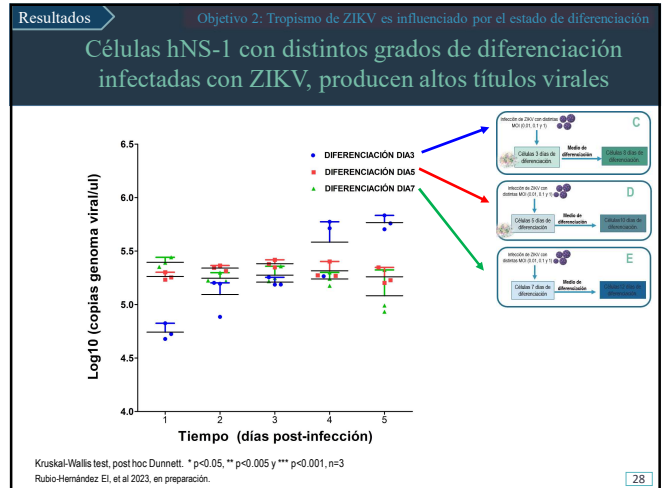
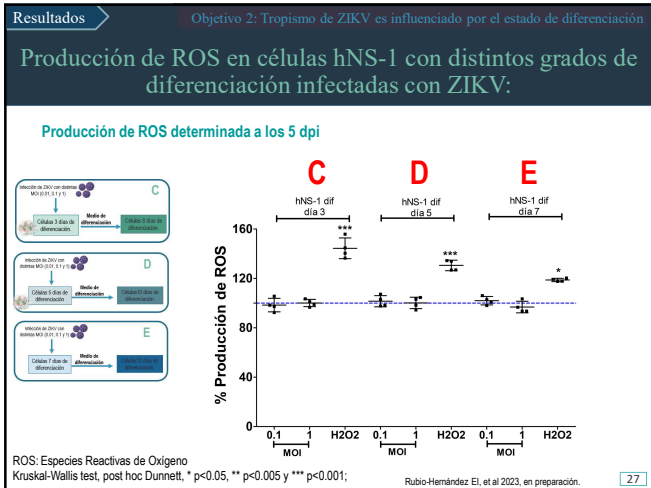
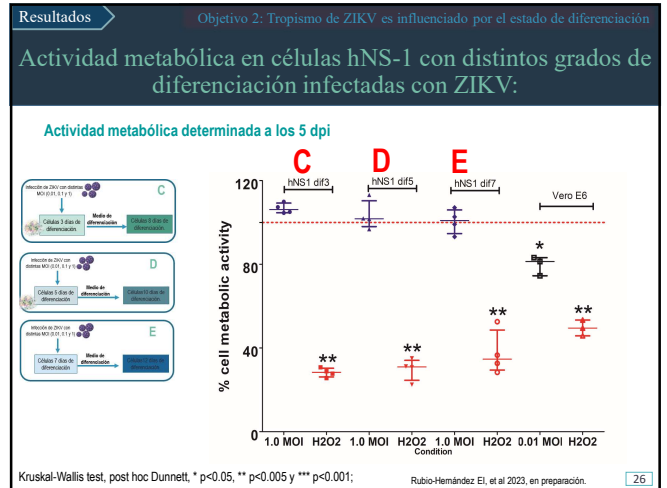
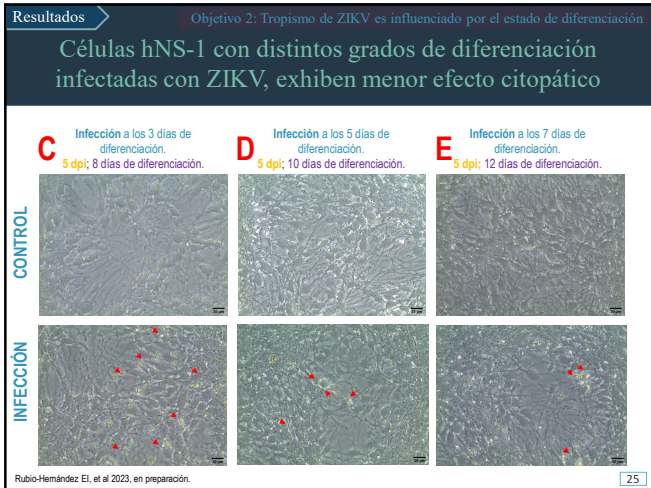
**Materiales y Métodos** Objetivo 2: Tropismo de ZIKV es influenciado por el estado de diferenciación

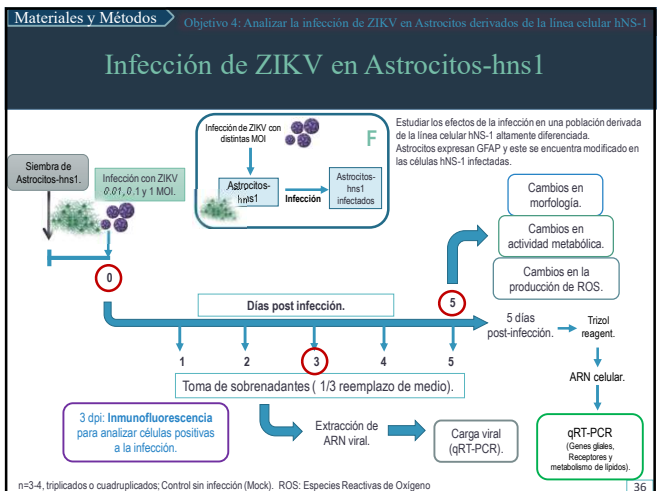
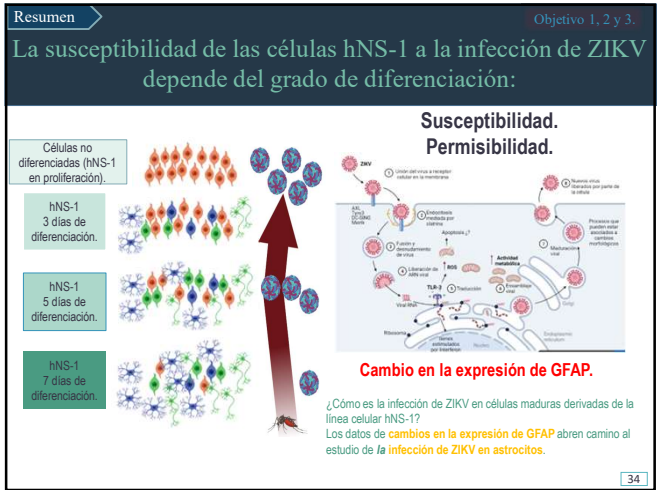
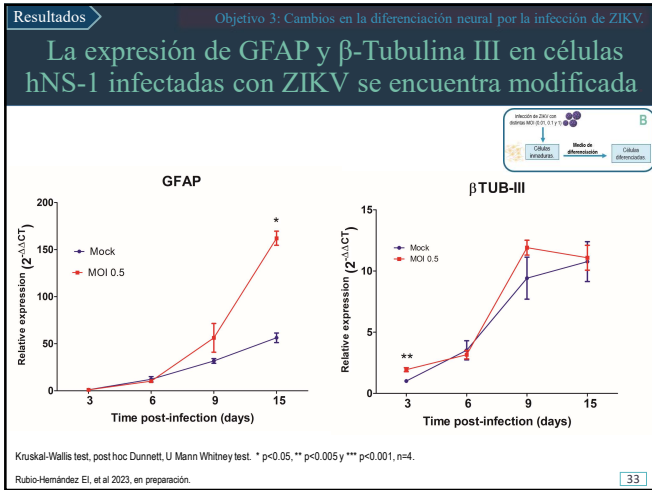
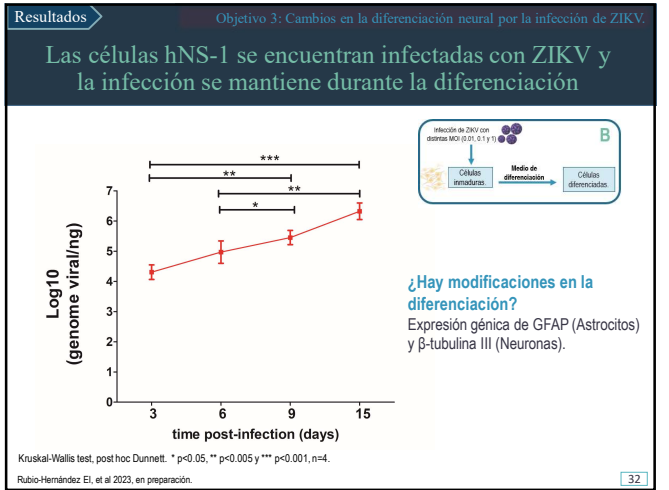
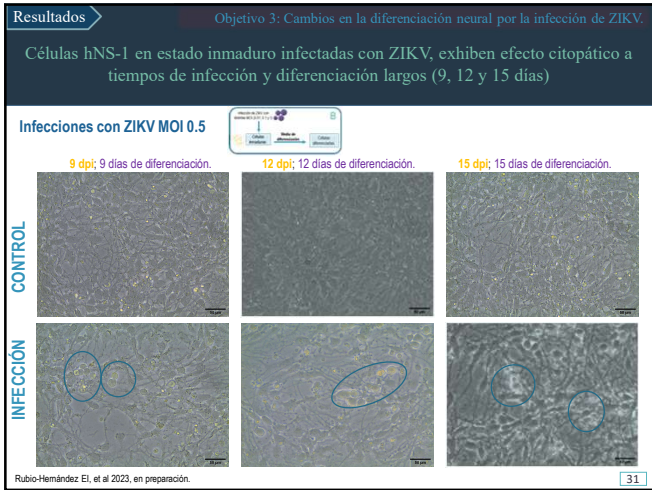
## Infección de ZIKV en células hNS-1 en un estado inmaduro:

Siembra de células hNS-1 → Infección con ZIKV 0.01, 0.1 y 1 MOI. → Cambios en morfología, actividad metabólica, producción de ROS. → 5 días post-infección. → Toma de sobrenadantes (1/3 reemplazo de medio). → Extracción de ARN viral. → Carga viral (qRT-PCR).

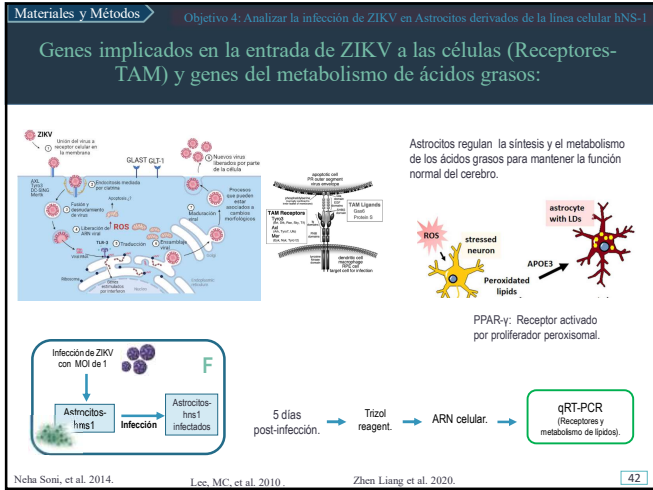
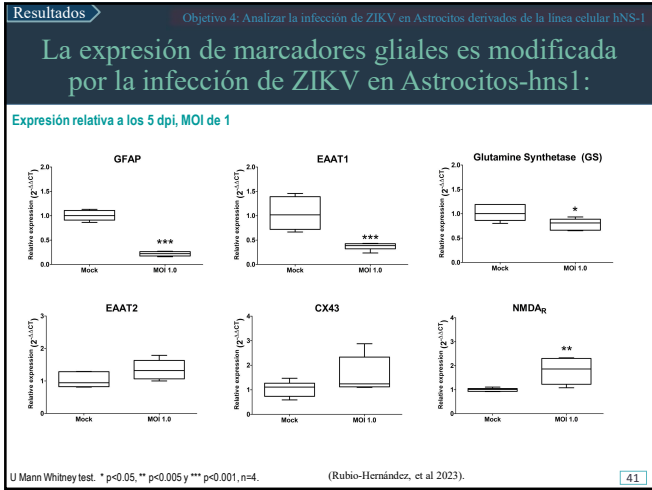
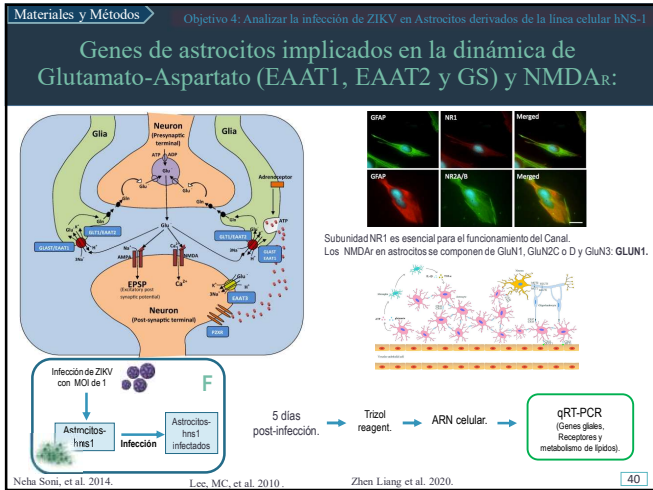
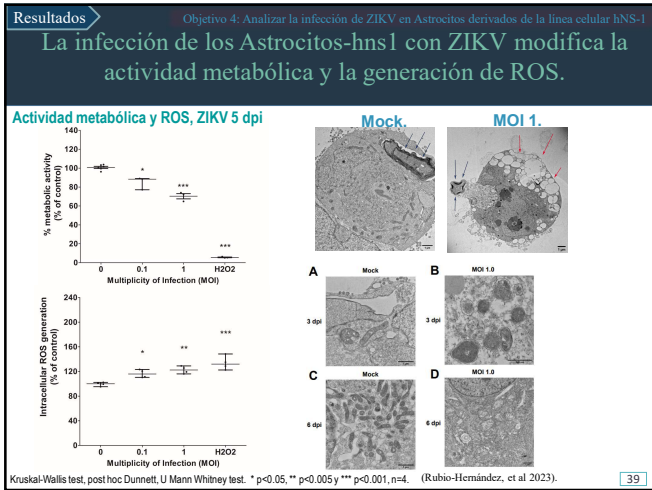
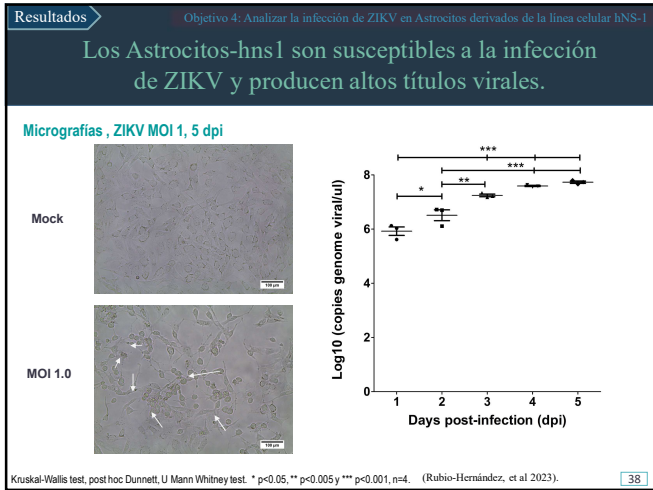
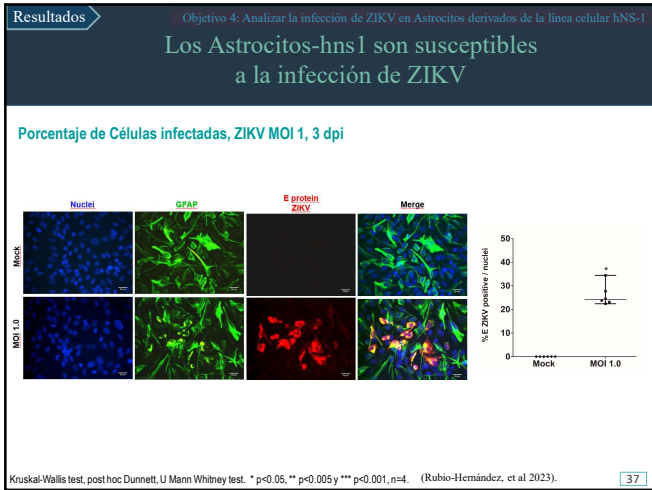
n=3-4, triplicados o cuadruplicados; Control sin infección (Mock). ROS: Especies Reactivas de Oxígeno







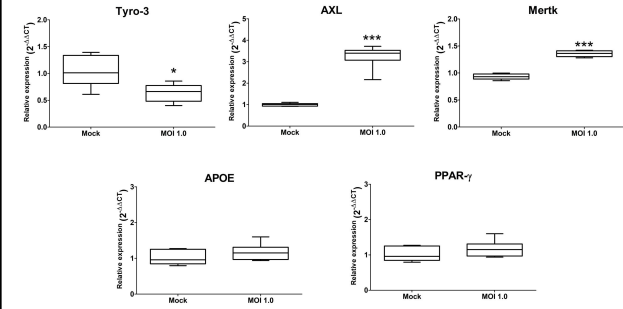




**Resultados** Objetivo 4: Analizar la infección de ZIKV en Astrocitos derivados de la línea celular hNS-1

La infección de ZIKV en Astrocitos-hns1 modifica la expresión de genes de la familia TAM y genes involucrados en el metabolismo lipídico:

Expresión relativa a los 5 dpi, MOI de 1

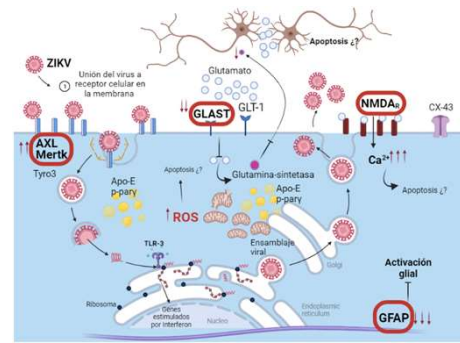


U Mann Whitney test. \* p<0.05, \*\* p<0.005 y \*\*\* p<0.001, n=4. (Rubio-Hernández, et al 2023, en prensa).

43

**Resumen** Objetivo 4: Analizar la infección de ZIKV en Astrocitos derivados de la línea celular hNS-1

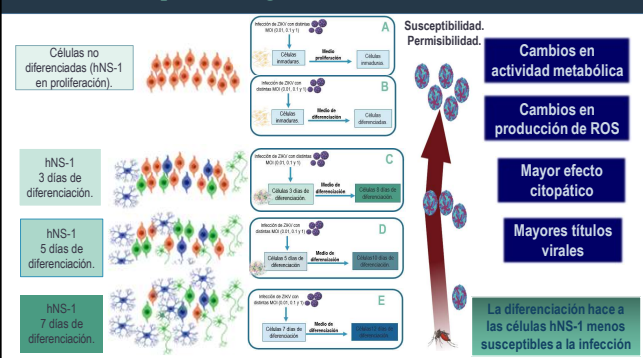
Los Astrocitos-hns1 son permisibles y susceptibles a la infección por ZIKV:



44

**Resumen** La susceptibilidad de las células hNS-1 a la infección de ZIKV depende del grado de diferenciación:

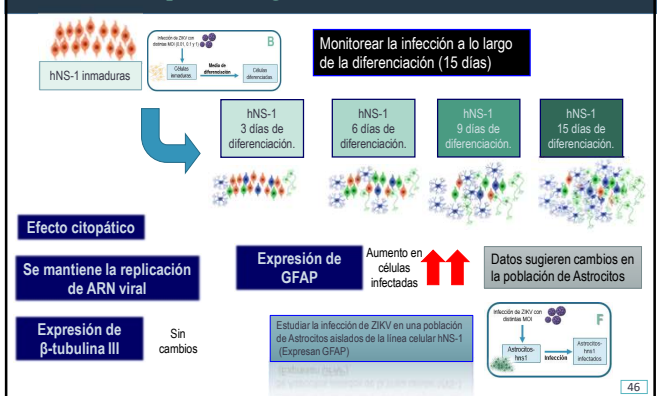
Células no diferenciadas (hNS-1 en proliferación). hNS-1 3 días de diferenciación. hNS-1 5 días de diferenciación. hNS-1 7 días de diferenciación.



45

**Resumen** La susceptibilidad de las células hNS-1 a la infección de ZIKV depende del grado de diferenciación:

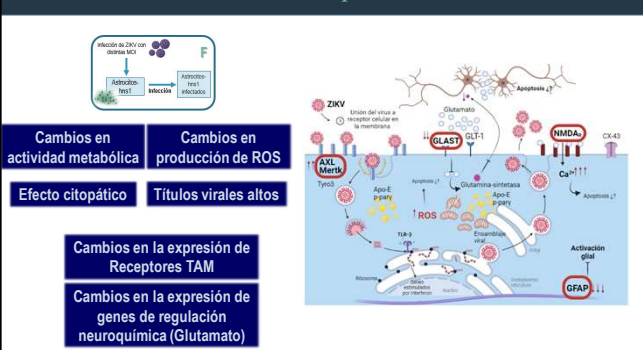
hNS-1 inmaduras. Monitorear la infección a lo largo de la diferenciación (15 días). hNS-1 3 días de diferenciación. hNS-1 6 días de diferenciación. hNS-1 9 días de diferenciación. hNS-1 15 días de diferenciación.



46

**Resumen** Los Astrocitos-hns1 son permisibles y susceptibles a la infección por ZIKV:

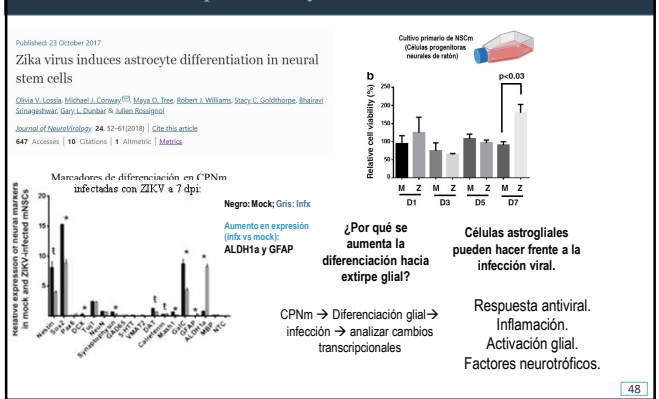
Cambios en actividad metabólica. Cambios en producción de ROS. Efecto citopático. Títulos virales altos.



47

**Discusión** Las células progenitoras neurales infectadas con ZIKV expresan mayores niveles de GFAP:

Zika virus induces astrocyte differentiation in neural stem cells. Published 23 October 2017. *Journal of Neurobiology* 24, 52-61 (2018).



48

**Discusión**

## La interacción entre distintas células modifica la infección por ZIKV:

DE GRUYTER | *NeuroImmune Pharmacol.* Ther. 2022; 20:22

Courtney Veilleux and Eliseo A. Eugenin\*

### Mechanisms of Zika astrocyte infection and neuronal toxicity

https://doi.org/10.1515/nip-2022-0004  
Received September 20, 2022; accepted October 2, 2022; published online October 21, 2022

Los efectos de la infección (muerte celular) difieren cuando se cultivan astrocitos y astrocitos en co-cultivo con neuronas.

49

**Discusión**

## Los Astrocitos son más susceptibles a la infección por ZIKV:

Frontiers | Open Access | Published 22 January 2023

### Zika virus infection leads to mitochondrial failure, oxidative stress and DNA damage in human iPSC-derived astrocytes

Elisa Flores-Ladra, Karina Karamillo, Carolina de Silva Souza Pedrosa, Letícia Rocha Quintino Souza, Gabriela Assis de Lencas, Thiago Martins Moreira, Maria de Castro Cavalcanti Gomes Ferreira, Gabriel Fontes de Almeida Neto, Klaus de Sena Silva, Cibele Silva, José Roberto Calvo, Nils Momeni-Chehres, Silvia Oliveira, Rodrigo Furtado Martins da Costa, Lúcia Siqueira Silva, Luiza Medeiros Faria, Adriana Melo, Andréia Jesus, Lúcia Chizzini, Marcos Mendes Moreira, Patrícia Pereira Gomes, Eduardo Corrêa de Figueiredo, Adriano Galvão, Helena Lúcia Barros & Simone Sampaio Rocha-Ferreira\*

Keywords: Astrocytes; Mitochondria; DNA Damage; Oxidative Stress

DOI: 10.3389/fnins.2022.1011111

50

**Conclusiones**

Las células progenitoras neurales son altamente susceptibles a la infección por ZIKV.

Cuando las células diferenciadas son infectadas, la susceptibilidad disminuye.

Al aislar una población altamente diferenciada, la susceptibilidad a la infección por ZIKV es alta.

Se sugiere que la interacción entre todos los tipos celulares neurales presentes en los distintos estadios de diferenciación modifican los patrones de infección.

51

**Conclusiones**

La muerte celular, la producción de ROS, el aumento de la actividad metabólica, pueden afectar los patrones normales de proliferación y migración, alterando la citoarquitectura del cerebro.

El estrés oxidativo se ha relacionado con un mayor riesgo de defectos del tubo neural.

Durante una infección congénita con ZIKV, se producen efectos en las células astrogiales, comprometiendo su buen funcionamiento.

El agotamiento de astrocitos puede conducir a déficits motores y pérdida neuronal causada por el estrés oxidativo.

52

**Perspectivas**

- ¿Qué factores vuelven permisivos y susceptibles a las células hNS-1 inmaduras y a los astrocitos?
- Analizar cambios en funcionalidad de las células infectadas con ZIKV.
- Realizar un sistema *in-vitro* que vincule más tipos celulares.
- Analizar los efectos sinérgicos de virus que se asocian a infecciones congénitas y con repercusiones en el neurodesarrollo.
  - Coinfecciones CMV y ZIKV.
  - Coinfecciones HHV-6 y ZIKV.

**Producción académica**

Manuscript Number: PONE-22-20681

Article Type: Research Article

Full Title: Astrocytes derived from Neural Progenitor Cells are susceptible to Zika Virus Infection

Corresponding Author: Claudio C. Castillo, PhD, Universidad Nacional de San Luis, San Luis, Argentina, CC-BY-NC-ND

Keywords: Zika virus, congenital infection, astrocytes, TAM receptors, lipid droplets, fibroblasts, cell death, gliosis

Abstract: Zika virus (ZIKV) was first isolated in 1947. Since its isolation until 2015, symptoms of ZIKV infection were limited to mild fever, rash, conjunctivitis, and muscle pain. During the epidemic in 2014, ZIKV infection caused children brain malformations in adults and neurological sequelae in children, including Guillain-Barré syndrome. The re-emergence of ZIKV has been related with neural progenitor cells (NPCs). Since astrocytes, neuronal stem cells, OPCs and astrocytes appear to be the most susceptible cells to ZIKV infection, we investigated the mechanisms by which we aimed to identify a subset of astrocytes derived from a human iPSC cell line. We analyzed how ZIKV infection affects astrocytes and determined that ZIKV infection leads to high cell death. It also led to changes in the expression of genes that regulate the entry of the virus into the cell. It then was proposed that a population of genes associated with changes in mitochondrial and DNA damage associated with production of reactive oxygen species could be involved in the ZIKV congenital infection. Therefore, which may help understand the pathogenesis of ZIKV-associated congenital disease.

Borrador de:

Zika virus differentially infects Human Neural Stem Cells according to their state of differentiation and dysregulates GFAP expression.

Rubio-Hernandez EF; Comas-García M, Martínez-Serrano A; Castillo CG.

Journal of NeuroVirology